A Computational Study of Compact Tension and Double Torsion Test Geometries

Sicelo Praisegod Goqo

Dissertation presented for the degree of Master of Science

Department of Mathematics and Applied Mathematics
Faculty of Science

University of Cape Town

August 2013

Supervisors: Prof Daya Reddy, Prof Robert Tait, Dr Sebastian Skatulla and Dr Thorsten Becker

Signature: Signed by candidate

Plagiarism Declaration

I know the meaning of Plagiarism and declare that all of the work in this document, save for that which is properly acknowledged, is my own.

LIST OF PUBLICATIONS

The following is the list of publications that were obtained from this thesis.

SUBMITTED CONFERENCE PUBLICATIONS

S.P. Goqo, S. Skatulla and T.H. Becker. Optimisation of the Double Torsion Geometry. *Proceedings of the Fifth International Conference on Structural Engineering, Mechanics and Computation (SEMC 2013)*. Research and Applications in Structural Engineering, Mechanics and Computation – Zingoni (Ed.). 2013 Taylor And Francis Group, London, ISBN 978-1-138-00061-2, pages 221 - 222.

CONFERENCE PRESENTATIONS

1. S.P. Goqo, R.B. Tait, S. Skatulla and D.B. Reddy. Application of Finite Element Methods, CFEM and XFEM, to Develop a Specimen Capable to Determine Fatigue Crack Growth Threshold. *Second African Conference on Computational Mechanics – an International Conference – AfriCOMP11*. Cape Town, South Africa (5 – 8 January 2011).

2. S.P. Goqo, R.B. Tait, S. Skatulla and T.H. Becker. Computational Study in Fracture Mechanics. *SANHARP 2nd Annual Postgraduate Conference*. I Themba LABS, Cape Town, South Africa (12 – 14 October 2011).

3. S.P. Goqo, S. Skatulla and T.H. Becker. Optimisation of the Double Torsion Geometry. *The Fifth International Conference on Structural*

Engineering, Mechanics and Computation (SEMC 2013). Cape Town (2 – 4 September 2013).

ACKNOWLEDGEMENTS

I would like to thank God for giving me courage to complete this project. If I were to single out everyone who contributed to making this project a success, it would require a number of pages; hence I have singled out those whom I thought contributed the most.

I also would like to thank my family and all my friends for their continuous support through all the years.

Professor Daya Reddy has supported me academically over the years, from the beginning up until the end of this project. He was the one who came with the idea of fracture mechanics. Thank you for all your assistance and guidance, and always wanting me to do well in my studies.

Professor Robert Tait was the one who came up with the idea of the project and how this would contribute to the future of fracture mechanics. Thank you for all your support and your readiness to discuss all the fracture mechanics problems that I encountered.

Dr Sebastian Skatulla has played the most significant part in this project. He has given me the most advice, and he has helped me to grow. In the modelling part, he gave me advice on everything that I needed for this work to be successful. Thank you for your patience during the hard times that I encountered.

Dr Thorsten Becker played a major role in the completion of the rest of this project. He introduced me, and was with me, at most of the conferences that I attended. He has helped me to grow in the research field, and all the constructive criticism has played an important part in the completion of this project.

The following is a list of people I would have liked to single out owing to their contribution and the advice that they gave me, which made this work a success. All of them have had an impact during the times I spent on completing this project:

CERECAM members, Kathryn Rosie, Hellmut Bowles, Greg Mitchell and Graham Inggs.

Keith Williams for the language editing.

Finally, I would like to thank SANHARP and CERECAM for financial support.

ABSTRACT

In the design of many engineering components subjected to cyclic or repetitive loading, fatigue is an ever-present challenge. The engineer often endeavors to design the structural or component system in such a way that the cyclic stresses are below a particular fatigue limit, or, in fracture mechanics terms, at stress levels below threshold. In the Paris formulation, fatigue threshold, ΔK_{th}, may be regarded as that value of cyclic stress intensity below which fatigue crack growth does not occur. For a particular material and environment, this threshold value, ΔK_{th}, is determined experimentally by monitoring growth of a crack (typically in a compact tension (CT) specimen) and continually reducing cyclic stress levels until the threshold condition is reached [1]. This procedure is very cumbersome and time-consuming, and this project rather considers the design of a fracture mechanics specimen geometry in which there is a **decreasing** stress intensity (with crack length) that facilitates determination of the threshold value simply at constant applied cyclic amplitude, and the crack length at which fatigue crack growth arrests.

Numerical methods provide a useful and cost-effective way to design such a specimen for easy experimental work and to assist in the fatigue design of components and structures. Numerical analysis can be used to overcome the cost and the amount of time spent on experimental work. Such an alysis was implemented here, where a very promising specimen has been designed using conventional finite element methods (CFEM) and extended finite element methods (XFEM). The CFEM is applied to study the stress intensity factors.

On the other hand, the dynamic modelling of fracture propagation results with XFEM, allows further understanding of design and assessment of this particular specimen. In particular, based on certain loading conditions, XFEM is applied in order to achieve the point of arrest of the stress intensity factors. This is the point of interest, especially in

fatigue fracture, since it provides a point known as the stress intensity fatigue threshold. Further, optimum specimen geometry, based on decreasing stress intensity factor specimen, was modelled using both methods.

CT specimen is the well-known and standardized specimen. This specimen was used to verify the FEM models. It consists of two see-through loading holes and a pre-included crack. The specimen is loaded in such a way that the crack will propagate in the direction perpendicular to the loads. This is one of the specimens capable of producing increasing stress intensity factors. As aforementioned, this specimen is probably the most widely used FM specimen and has proven very effective in the laboratory testing environment. Therefore, it is used in this project to verify the models.

The FEM model is applied to the CT specimen to study the SIF and the results are verified using analytical methods. Further, the SIF equation is derived and solved analytically to obtain a desired decreasing SIF specimen. The resulting specimen is then investigated using FEM.

On the other hand, the Double Torsion (DT) geometry is a test specimen configuration that facilitates for fracture investigations in highly brittle materials and is well-known to produce a stress intensity factor that is independent of crack length. This feature allows for the propagation of relatively long cracks in a highly controlled manner in exceptionally brittle materials. However, the DT geometry is yet to be standardised and, to date, many questions remain regarding optimal specimen dimension, load-point deflections, and out-of-plane deformations. This project also aims to investigate the DT geometry using the conventional Finite Element Methodology in order to obtain an **optimum** specimen geometry that can be utilised in fatigue threshold and other fracture-mechanics-related investigations.

A total number of 45 specimen geometries were investigated. The focus was on the thickness, length and width. Different observations were compared in order to predict an optimum geometry.

TABLE OF CONTENTS

LIST OF TABLES

LIST OF FIGURES

LIST OF SYMBOLS

B	Geometry thickness
a	Flaw size of the geometry
W	Width of the geometry
K_{IC}	Fracture toughness
σ_y	Yield stress
σ	Remote stress
j	J – integral
K	Stress Intensity Factor
Y	Dimensionless parameter
ΔK	Change in Stress Intensity Factor
K_{max}	Maximum Stress Intensity Factor
K_{min}	Minimum Stress Intensity Factor
K_C	Critical S tress I ntensity F actor f or p lane stress conditions
K_{IC}	Critical S tress I ntensity F actor f or p lane strain conditions
r	Radius
K_I	Mode I Stress Intensity Factor
K_{II}	Mode II Stress Intensity Factor
K_{III}	Mode III Stress Intensity Factor
θ	Angle created by the radius
G	Energy release rate

E	Young modulus
C	Compliance
h	Height
P	Load
d	Thickness
L	Length
W	Width
W_m	Moment arm
Ψ	Thickness correction factor
c	Crack front inclination
b	Breadth

ABBREVIATIONS

FM	Fracture Mechanics
PBMR	Pebble Bed Modular Reactor
SIF	Stress Intensity Factor
CT	Compact Tension
DT	Double Torsion
DTDCB	Decreasing T apered Double C antilever Beam
TDCB	Tapered Double Cantilever Beam
FE	Finite Elements
LEFM	Linear Elastic Fracture Mechanics
FEM	Finite Element Method
CFEM	Conventional Finite Element Method
XFEM	eXtended Finite Element Method

CHAPTER ONE

INTRODUCTION

The fracture of materials may be understood as the phenomenon where the presence of a flaw, or a crack, weakens the material to such an extent that failure can occur at loads significantly lower than the material's strength. Fracture can result in catastrophic failures that can have severe consequences, such as the loss of life. Classic examples of catastrophic fracture failures include the Liberty ships which were built during the Second World War. These ships were considered to be of superior design owing to the then newly developed welding technology, which enabled much faster ship construction. More than 4 000 of these ships were built before and after World War I [2]. A quarter of these experienced brittle fractures (even though the ship material was an inherent ductile material - mild steel) [3]. An investigation concluded that cracks had propagated through the welding in the ship's hull over time to a critical length, resulting in the catastrophic failure in which the ship broke in half, Fig (1.1). An additional example is the Comet aircraft disaster of 1954 – a tragic airplane crash. The Comet aircraft was again a novel design of the time; however, it experienced catastrophic failure owing to a lack of understanding of the fracture phenomenon. Fatigue cracks, caused by repetitive loading, initiated at the rivet holes in the fuselage near the passenger windows, which, over time, propagated to a critical length to result in a sudden catastrophic rupture of the fuselage.

Fortunately, in this day and age, we understand the phenomenon of fracture, and we can design or assess components and structures against such catastrophic failures. One of the tools that can be used to explain and predict such failures is Fracture Mechanics (FM). First developed by A. A. Griffith, it enables an explanation of the brittle type failures in

ductile materials [4]. Since then, Fracture Mechanics has been used to explain different types of failures in various materials.

Figure 1.1. Liberty ship breaking completely in two [2].

As technology has improved over time, new complex structures have required special precautions when assessing structures for fracture failures. To design and assess components and structures against fracture, using FM, requires the knowledge of fracture parameters. These parameters describe the inherent behaviour of the materials, which can be determined through standardised testing procedures. Typically, these testing procedures make use of small specimens in controlled laboratory conditions to obtain the material's fracture properties that are then applied to full-scale structures in industry [5]. For example, owing to repetitive loads experienced by structures, fatigue fracture, which results in failure, may be experienced.

The fatigue stress intensity threshold (fatigue threshold) ΔK_{th} is an important design parameter in fracture mechanics. If it is properly applied to structures, it ensures that the structure will not propagate a fatigue crack. This value is also obtained in the laboratory from the small test specimens.

Another example is found in the brittle materials, typically in the nuclear reactor. The nuclear graphite is used as a neutron moderator within a nuclear reactor [6]. One example of a nuclear reactor is the Pebble Bed Modular Reactor (PBMR), (see more discussion in [6]). This is the type of reactor that uses graphite components which form a part of inner core structure. Nuclear graphite is a type of brittle material, and therefore there is a special need to understand its fracture properties to prevent catastrophic failure. Similarly, when testing, small specimens are utilized to understand the nuclear graphite.

However, these tests have limitations, especially for highly brittle materials (such as glass, concrete and nuclear graphite) and can result in erroneous results if certain test conditions are not met with respect to the material used and loading conditions. It is known that, in brittle materials, limited non-linearity may occur at the crack tip [1]. This can result in rapid and uncontrolled crack propagation, especially when high loads are applied. Hence, no fracture data can be measured. Different test approaches are needed in order to be able to measure brittle material's fracture parameters.

Such types of material behaviour require special testing geometries that allow for the investigation of the parameters that are used to assess the material's structural integrity. For the fatigue-threshold investigations, an ideal laboratory specimen would allow for testing conditions in which the fatigue threshold can be simply and accurately determined. A simple approach would be to have a specimen that has a crack length with decreasing Stress Intensity Factor (SIF). In such a specimen, the crack would propagate under fatigue loading until the material's fatigue threshold SIF is reached [7].

Consequently, the material's threshold SIF can be simply determined. In quasi-brittle materials, such as Nuclear Graphite, ideal test conditions would allow for stable and controlled crack conditions that enable the investigation of the fracture parameters [6].

Both of these idealized conditions require a special condition, which is that of a constant or decreasing SIF with crack length. Typically, this is not the case for standard laboratory test specimens, such as the Compact Tension (CT) specimen, where the SIF increases with crack length. Therefore, this project aims to investigate two specimen geometries that allow for such special conditions:

1. A crack length decreasing SIF (allowing for fatigue threshold investigations).
2. A constant stress intensity factor specimen (allowing for investigations of brittle materials).

1.1 Fracture Mechanics Approach

All structures contain flaws, either occurring naturally or initiated in service [8]. These flaws may exist owing to welding flaws, porosity, or microscopic crack-like flaws. As aforementioned, FM is a tool which may be utilised to predict and avoid potential catastrophic failures of structures which contain such flaws. FM uses methods of solid mechanics to characterise and study fracture properties of materials in order to assess structures or components with flaws or cracks. It provides a means for understanding the relationship between stress, flaw size and material fracture toughness, known as the triangle of integrity (as shown in Fig. (2.1),with more discussion in Chapter 2).

1.2.1 FRACTURE TOUGHNESS TESTING

During fracture toughness investigations, a crack is introduced into a specimen and propagated under closely controlled loading conditions [9]. This allows for the calculation of the stress intensity factor (SIF), which describes the stress calculated near the crack tip. At the critical point, i.e. at the point of catastrophic failure (either owing to the crack length or the load reaching a critical point), the stress intensity factor is the measure of the fracture toughness.

There are several types of specimen geometries that have been used to evaluate the fracture toughness of materials. These include the single-edge notched, three-point bending specimen and the compact tension specimen [8]. However, the use of these specimens can prove difficult when testing highly brittle and quasi-brittle materials, since they do not facilitate for stable crack propagation conditions. The specimens have an increasing SIF (with crack length) which, when a highly brittle material is tested, results in sudden breaks. As such, alternate specimen geometries are required that accommodate brittle and quasi-brittle materials. Such specimens should ideally allow for an increasing or decreasing SIF.

Testing procedures have been developed that allow for such conditions; however, they have been reported to be inaccurate and therefore require further analysis [6,7]. One of the aims of this project is to investigate a novel specimen geometry that allows for stable test conditions, especially in brittle materials. The interest lies in contributing to the standardisation of such specimen geometry, i.e., the double torsion geometry (discussed in detail in Chapter 3). The study aims to utilise numerical methods as the basis of the investigation.

1.2.2 Decreasing and Constant Stress Intensity Factor Specimen

The first specimen geometry to be investigated is the geometry that is capable of producing decreasing SIF. This means that, as the SIF decreases, stable crack growth may be achieved, and hence the fatigue threshold SIF value (where crack can or cannot grow) may be determined. This is particularly important for fatigue threshold investigations.

The second proposed geometry investigated is a constant stress intensity factor specimen. The Double Torsion (DT) specimen has been utilised for brittle materials, and it allows for a constant SIF (i.e. independent of crack length). This results in slow, stable and controlled crack propagation, and hence the fracture toughness value can be determined. The fracture toughness value can also be determined using other geometries, e.g. chevron notch, CT [1]. However, we cannot observe the fracture mechanisms.

1.3 Computational Modelling

Numerical methods provide a useful and cost-effective way to design and assess fracture mechanics specimens for easy experimental work and to assist in the fatigue design and characterization of components and structures. Numerical analysis can be used to overcome the cost and the amount of time spent on experimental work.

In this project, the Finite Element modelling that was undertaken in this work utilised the commercial package Abaqus/STANDARD version 6.10 [10].

There are different ways to verify the models. Since the CT specimen has been standardized [11], the first models were compared to the known analytical solutions. The

CT specimen was modeled first, and then it was compared to the analytical solutions. Once the model had been verified, it was then applied to the other geometries.

On the other hand, the DT model solution convergence was obtained with the use of the contour integral convergence method using elements surrounding the crack tip [10]. Once the convergent solution is obtained, it may then be used to find the solutions. In addition, the analysis was performed on the DT models where the analytical K_{IC} value was used as the reference to calculate the SIF accurately.

1.4 Aims of the project

The aims of this project can be split into two sections, namely to investigate a specimen geometry that allows for a decreasing SIF (allowing for fatigue threshold investigations), and a specimen that allows for a constant (crack-length independent) SIF (allowing for brittle material investigations). The former objective aims to develop a modified compact tension specimen geometry that allows for a decreasing SIF, to facilitate fatigue threshold investigations. This investigation is undertaken using the conventional finite element method (FEM) and extended finite element method (XFEM). The FEM method was applied in order to model decreasing SIF, and the XFEM was applied in order to obtain the fatigue point where no crack propagation is observed, based on certain loading conditions.

Both methods facilitate the investigation and the design of fracture mechanics specimen in which there is a decreasing stress intensity (with crack length) that facilitates determination of the threshold value simply at constant applied cyclic amplitude, and the crack length at which fatigue crack growth arrests

The latter aims to assess the constant stress intensity factor regime of the DT specimen and follows on the recommendations made by Becker et al. [6]. The investigation is undertaken using the conventional finite element method (FEM). The DT geometry is investigated using the conventional Finite Element Methodology in order to obtain an optimum specimen geometry that can be utilised in fatigue threshold and other fracture-mechanics-related investigations

1.5 Format of the Thesis

A more theoretical background review of fracture mechanics and a literature review of both the compact tension and the double torsion specimen are presented in Chapter 2. This chapter includes an introduction into finite element method. Furthermore, the literature review of the fracture mechanics approach is provided.

Chapter 3 gives a description of the specimens utilised in this project - the Compact Tension specimen and the Double Torsion specimen. Also, the decreasing SIF specimen is introduced in this chapter.

Chapter 4 describes the method utilised for the modelling process. More details of Abaqus implementations are given in more detail in Appendix A (Compact Tension and Decreasing Tapered Double Cantilever Beam) and Appendix B (Double Torsion). This is followed by results and discussion on both geometries in Chapter 5.

Chapter 6 provides more discussion of the results. Chapter 7 concludes the thesis and provides future project recommendations.

CHAPTER TWO

LITERATURE REVIEW

This chapter aims at providing a brief background and overview of fracture mechanics methodology that is relevant to this project. Having these in mind, it is appropriate to divide the chapter into three sections. The first section provides the Fracture Mechanics overview in detail. This is followed by the second section where the background description of the specimens that form the main aim of this work is provided. Finally, the Finite Element modelling approach theory description is provided as the third section.
It is worth noting that the sections that we discuss will only be those that are relevant to this project. For further reading, the reader is directed to the literature and the references that are provided in this work.

2.1 Fracture Mechanics Methodology

The study of Fracture Mechanics (FM) is of fundamental importance in the study of the mechanics behind the crack propagation. Structural integrity assessment, material and structural failures, as well as the fatigue life predictions are only but a few areas in which fracture mechanics plays a major role in the study of the propagation of cracks. An example of the cause of crack propagation is the cyclic, repeated loading of a structure [12,1]. Such loading is referred to as fatigue crack propagation, which is discussed in more detail in section (2.1.8).

Constant loading is another cause of crack propagation in a material [1]. We focus attention on crack propagation that is caused by the constant loading conditions, especially in the energy balance approach section (2.1.3).

2.1.1 LINEAR ELASTIC FRACTURE MECHANICS (LEFM)

Linear Elastic Fracture Mechanics (LEFM) is the basic theory of fracture mechanics that assumes that the crack tip experiences no plasticity during the opening of the crack, and that the force-displacement relationship is linear. Thus, the material with relatively low plasticity can be analyzed using the theory behind LEFM. Some of the few assumptions during the application of this theory are:
The material is linear elastic, except at the crack tip region where inelastic behaviour has been observed [1,13], and isotropic (same properties everywhere in the material). Most geometries are analyzed using plane strain assumption. This assumption must be validated using Equation (2.1) [1]

$$B,\ a,\ \frac{W}{2} \geq 2.5 \left(\frac{K_{IC}}{\sigma_y}\right)^2 \tag{2.1}$$

where B is the geometry thickness, a is the flaw size of the geometry in question, W represents the width of the geometry, K_{IC} is the fracture toughness and σ_y is the yield stress in the geometry.

LEFM assists in studying FM parameters which help us answer the structural integrity question. For example, we can determine why structures fail using the FM parameters. Two of the useful and most studied parameters in FM are fatigue threshold and fracture toughness, which are properties that will allow us to determine the failure of materials

which contain cracks. One of this project's interests is in the understanding of the fracture toughness parameter.

The LEFM method is based on either energy calculations or stress intensity factor calculations. Both methods are related and provide identical results when applied in FM. Before we look at the two methods, it is important that we understand the basic LEFM characteristics; to name the few, the triangle of integrity and the fracture toughness.

2.1.2 TRIANGLE OF INTEGRITY APPROACH

Fracture mechanics can be practically applied in most situations where any two of the three properties of remote stress applied to the system σ, i.e. flaw size or crack length a and fracture toughness (K_{IC}, COD, j), (known as triangle of integrity), Fig. (2.1), are known. If any two of the three are known, the third can be calculated using Equation (2.2)

$$K = Y\sigma\sqrt{\pi a} \tag{2.2}$$

where Y is the dimensionless parameter depending on the specimen and crack geometry and K is the stress intensity factor.

Under cyclic, repeated loading, stress intensity factor is expressed as $K = \Delta K = K_{max} - K_{min}$. If $\Delta K \geq K_{IC}$, fast fracture occurs. The stress intensity factor, K, is the measure of the magnitude of the elastic stress field at a crack tip, which is under stress described by Equation (2.2).

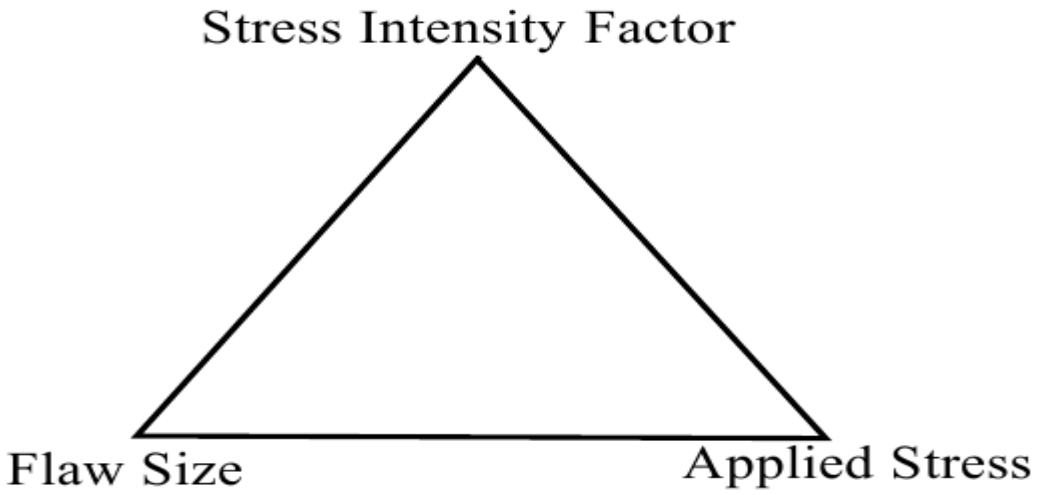

Figure 2.1. The triangle of integrity, denoting a relationship between flaw size (a), applied stress (σ) and the SIF (K). Note that the Stress Intensity Factor provides us with the fracture toughness.

2.1.3 FRACTURE TOUGHNESS

The stress field near the crack tip is calculated using the theory of elasticity, which is discussed in detail in the work of [14]. This theory focuses on stress intensity factor K, which describes the magnitude of the elastic crack tip stress field.

On the other hand, fracture toughness, by definition, is the resistance of material to undergoing failure. Under conditions of limited crack tip plasticity, the parameter governing the tensile fracture, called mode I, in Fig. (2.4), is related to the critical stress intensity, either K_C (plane stress conditions) or K_{IC} (plane strain conditions).

The critical stress intensity is the material-dependent factor $K_{IC} = K_{IC}(\text{material})$. The stress intensity factor K should not exceed $K_{IC,}$ the critical stress intensity, i.e. $K < K_{IC}$,. If it does occur, then failure will occur. K_{IC} can be considered a material property characterizing the crack resistance, and it is therefore called the plane strain fracture toughness. Thus, the same value of K_{IC} should be found by testing specimens of the same material with different geometries and with critical combinations of crack size, shape and fracture stress. The knowledge of K_{IC} obtained under ASTM standard conditions [11] can be used to predict failure for different combinations of stress and flaw size and for different geometries.

The K_{IC} value can be obtained at the crack tip from the stress parameters shown in Fig. (2.2). At the crack tip, the stress field can be expressed as a product of $\frac{1}{\sqrt{r}}$ and a function of θ with a scaling factor

$$\lim_{r\to 0} \sigma = \frac{K_I}{\sqrt{2\pi r}} f(\theta) \qquad (2.3)$$

where f is a function of polar coordinate which can analytically be defined, σ stress at the crack tip, K_I is the mode I SIF and θ is the angle created by the radius r at the crack tip.

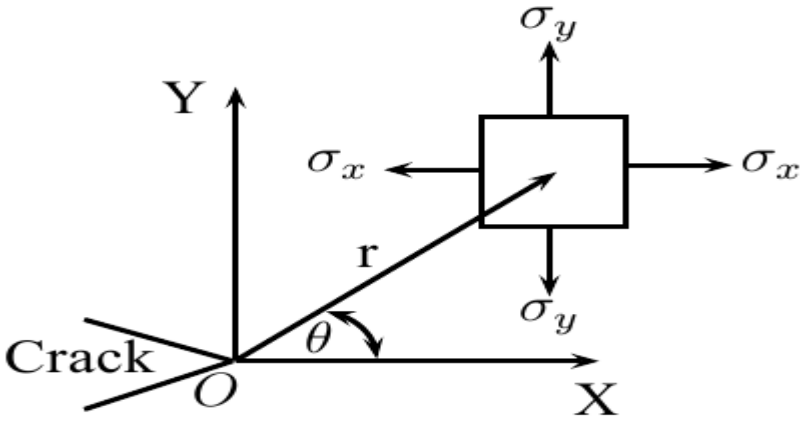

Figure 2.2. Crack tip showing stresses in the x and y directions.

There are two approaches that are used to evaluate the K_{IC} value at the crack tip - the energy balance approach and the stress intensity factor approach. Both approaches approximate stresses by the stress intensity factor values. These values are then used to obtain the required K_{IC} value.

2.1.4 THE ENERGY BALANCE APPROACH

The energy balance approach was proposed by Griffith in the early 1920s [15]. The basic idea behind the energy balance approach lies in the gaining and losing of energy by an object or species that is subjected to loadings. Griffith proposed that the crack extension $U_p$causes the loss in potential energy during cracking of the material, and this is opposed by the increase in surface energy owing to the increase in surface area U_γ. It should be noted that this approach is only applicable to brittle materials, and it also does not account for the stored energy in the system [1]. Nonetheless, the Griffith approach can be followed as one of the basic approaches in FM. The method formulation is as follows:
Consider an infinite plate of unit thickness containing a through-thickness crack of length $2a$ and that is subjected to a boundary stress σ applied at infinity, see Fig. (2.3). The total energy U of the cracked plate can be written as:

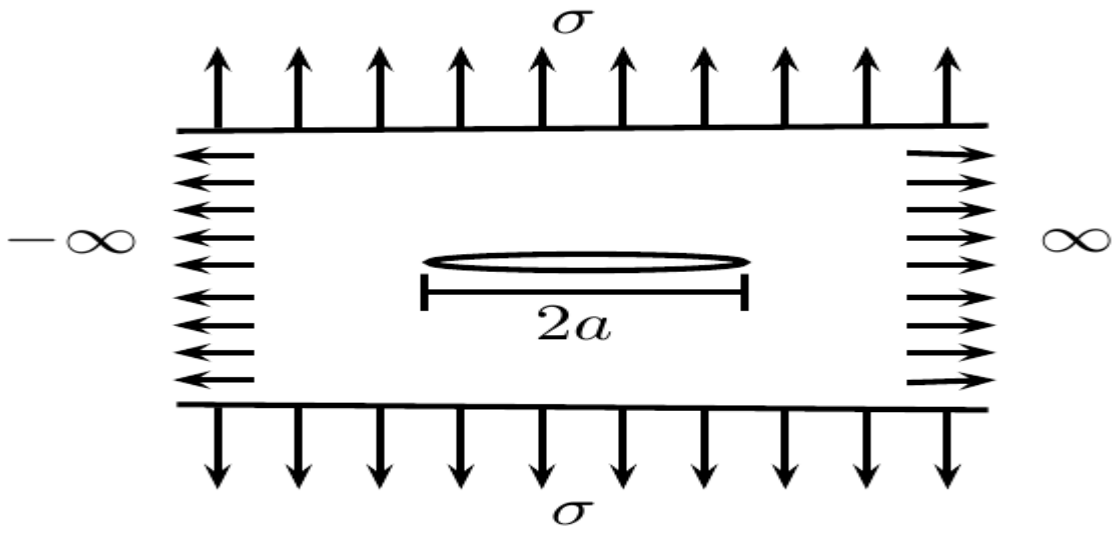

Figure 2.3. An infinite plate containing a center crack of length $2a$.

$$U = U_0 + U_a + U_\gamma - F \tag{2.4}$$

where,

$U_0 = \int_A \frac{\sigma^2}{2E}$ = constant is the elastic energy, where A is the surface area of concern and E is the young modulus.

$U_a = \pm\pi\frac{\sigma^2 a^2}{E}$ is the elastic strain energy release caused by the introduction of a crack in the plate and the relaxation of the material above and below the crack,

$U_\gamma = 2(2a\gamma_e)$ is the elastic surface energy, γ_e is the elastic strain work, and

F is the work done by the external forces.

When the fixed grip or constant displacement load is applied, there are no external forces acting, and the change in elastic energy is negative. Therefore, the total energy U of the crack plate is:

$$U = U_0 + U_a + U_\gamma = \int_A \frac{\sigma^2}{2E} - \pi\frac{\sigma^2 a^2}{E} + 4a\gamma_e \quad (2.5)$$

If we consider a crack at equilibrium, i.e. $\frac{dU}{da} = 0$, then $\frac{dU_0}{da} = 0$ since U_0 is constant. Therefore,

$$\frac{d}{da}\left(-\pi\frac{\sigma^2 a^2}{E} + 4a\gamma_e\right) = 0 \quad (2.6)$$

which can be simplified easily to

$$\sigma\sqrt{a} = \frac{2E\gamma_e^{\frac{1}{2}}}{\pi}. \quad (2.7)$$

The Griffith results only account for brittle material, since no plasticity appears in Equation (7). For interest, what happens if we take into account the plasticity occurring during loading? This question was answered by Irwin, who presented a modification to the Griffith theory in 1948.

If the resulting equation is rearranged such that we have $\frac{\pi\sigma^2 a}{E} = 2\gamma_e$, the left-hand side of this equation is called the energy release rate, G, and it represents the elastic energy per unit crack surface of the plate. The right-hand side represents the elastic crack surface of crack surfaces for plane stress and plane strain. This is the energy for incremental crack resistance [1,15].

The modification by Irwin suggested that the Griffith theory for ideally brittle materials could be modified and applied to both brittle and ductile (with plasticity) materials.

This modification was a realization by Irwin that a material's resistance to crack extension is equal to the sum of the elastic surface energy and the plastic strain work, γ_p,

$$\frac{\pi\sigma^2 a}{E} = 2(\gamma_e + \gamma_p) \quad (8)$$

The left-hand side of equation (8), assigned to G, is related to the SIF as $G = \sqrt{JK}$, where J is the J-integral, which will be discussed shortly in Section (2.1.7)

2.1.5 STRESS INTENSITY FACTOR (SIF) APPROACH

The study of fracture mechanics helps engineers to understand how mechanical systems behave, and eventually fail, owing to the initiation and progression of cracks. One of the parameters that they use to understand crack growth is the stress intensity factor, K, in FM. It was developed in 1950's by Irwin. He showed that the stress at the crack tip can be represented as:

$$\sigma_{ij} = \frac{1}{\sqrt{2\pi r}}\left(K_I f^I{}_{ij}(\theta) + K_{II} f^{II}{}_{ij}(\theta) + K_{III} f^{III}{}_{ij}(\theta)\right) \quad (2.9)$$

where f_{ij} is the geometric factor and r, θ are the cylindrical polar coordinates defining the position of an element ahead of the crack tip. K is a constant known as the stress intensity factor which gives the magnitude of the elastic stress field, and K_I, K_{II} and K_{III} denote the modes of crack surface displacements depicted in Fig. (2.4). From now on, the stress intensity factors will be referred to as SIF.

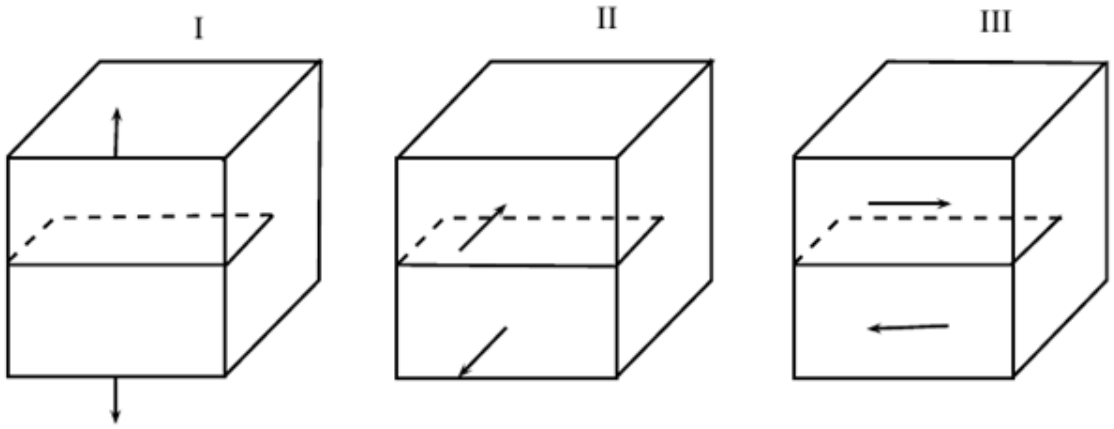

Figure 2.4. Modes of crack opening denoting loads represented by arrows. I, II and III represents modes I, mode II and mode III.

SIF also shows how stresses in the region near the tip of the crack are affected by the applied load and the crack geometry for different modes of loading. This relationship was discussed earlier, and it is represented in Equation (2.2). Mode I is the opening mode where crack surfaces move directly apart, Mode II is in-plane sliding of cracks, and Mode III is out-of-plane sliding of cracks. Most of the FM work has been devoted to Mode I owing to its simplicity. We are going to follow the same approach in this work.

2.1.6 DETERMINATION OF K_I - ANALYTICAL APPROACH

When the geometry is simple, analytical methods can be used to determine the SIF. For complex domains, other approaches, such as numerical methods or experimental methods, may be used.

In the case of an analytical approach, we present in detail the derivation of the Mode I stress field equations, originally developed by Westergaard [1]. The following pages follow this canonical derivation closely.

Since the SIF K describes the magnitude of the elastic crack tip stress field, we can derive SIF using stresses σ_x, σ_y and τ_{xy} by using the equilibrium equations of stress:

$$\sigma_x = \frac{\partial^2 \varphi}{\partial y^2} \tag{2.10}$$

$$\sigma_y = \frac{\partial^2 \varphi}{\partial x^2} \tag{2.11}$$

$$\tau_{xy} = \frac{\partial^2 \varphi}{\partial x \partial y} \tag{2.12}$$

where $\varphi(x, y)$ is the function that fulfils the equilibrium equations of stresses. For the compatibility equation of strains, we can derive the fourth order partial differential equation called the bi-harmonic equation:

$$\nabla^4 \emptyset = \nabla^2[\nabla^2 \emptyset] = 0 \tag{2.13}$$

where $\emptyset$ is any real function that depends on x and y variables. Functions that fulfil the bi-harmonic equations are called Airy stress functions. An infinite bi-axially loaded plate problem containing a crack, Fig. (2.3), can be solved using the complex stress function introduced by Westergaard:

$$\emptyset = Re\overline{\overline{\emptyset}}(z) + y\, Im\overline{\emptyset}(z) \tag{2.14}$$

subject to the following boundary conditions:
$\sigma = 0$, for $-a < x < +a$ and $y = 0$.

$\sigma \rightarrow \sigma_{\infty,}$ as $x \rightarrow \pm\infty$

$\sigma_y \rightarrow \infty,$ i.e. it has singularities at $x = \pm a$.

where an alytical function $\emptyset(z)$ i s t he f unction of complex v ariables $z(x + iy),$ which satisfy the boundary conditions for the plate, and $\overline{\emptyset}$ and $\overline{\overline{\emptyset}}$ are the first and second order integrals [16].

It has been proved that the real and imaginary parts of such an analytical function fulfil the bi-harmonic equation. Therefore, analytical functions similar to Equation (2.14) can be used as the stress function.

The well-known Cauchy-Riemann equations in complex analysis state that

$$\frac{\partial(Re\, f(z))}{\partial x} = \frac{\partial(Im\, f(z))}{\partial y} \tag{2.15}$$

and

$$\frac{\partial(Re\, f(z))}{\partial y} = -\frac{\partial(Im\, f(z))}{\partial x}. \tag{2.16}$$

We can find expressions for stresses σ_x, σ_y and τ_{xy} by taking derivatives of (2.14) and obtain:

$$\sigma_x = Re\, \emptyset(z) - y\, Im\, \emptyset(z)$$
$$\sigma_y = Re\, \emptyset(z) + y\, Im\, \emptyset(z)$$
$$\tau_{xy} = -y\, Re\, \emptyset'(z) \tag{2.17}$$

where $\emptyset'(z)$ is the first order derivative. The function $\emptyset(z)$, which satisfies the boundary conditions, has been shown [1] to be:

$$\emptyset(z) = \frac{\sigma}{\sqrt{1-\frac{a^2}{z^2}}}. \tag{2.18}$$

If the origin is translated to the crack tip, taking $\eta = z - a$, the stress function becomes:

$$\emptyset(\eta) = \frac{\sigma}{\sqrt{1-\frac{a^2}{(\eta+a)^2}}} = \frac{\sigma(a+\eta)}{\sqrt{(a+\eta)^2-a^2}} \tag{2.19}$$

For $\eta \ll a$, taking the first order approximation in a series expansion and using polar coordinates (r, θ), we get:

$$\emptyset(\eta) = \frac{\sigma\sqrt{a}}{\sqrt{2r}} e^{-\frac{1}{2}i\theta} \tag{2.20}$$

or

$$\emptyset(\eta) = \frac{\sigma\sqrt{\pi a}}{\sqrt{2\pi r}} e^{-\frac{1}{2}i\theta}. \tag{2.21}$$

We can now take $Re\ \emptyset(\eta)$, $Re\emptyset'(\eta)$ and $Im\emptyset'(\eta)$ and substitute in Equations (2.17) resulting in:

$$\sigma_x = \frac{\sigma\sqrt{\pi a}}{\sqrt{2\pi r}} \cos\left(\frac{\theta}{2}\right)\left(1 - sin\left(\frac{\vartheta}{2}\right) sin\left(\frac{3\vartheta}{2}\right)\right), \tag{2.22}$$

$$\sigma_y = \frac{\sigma\sqrt{\pi a}}{\sqrt{2\pi r}} \cos\left(\frac{\theta}{2}\right)\left(1 + sin\left(\frac{\vartheta}{2}\right) sin\left(\frac{3\vartheta}{2}\right)\right), \tag{2.23}$$

$$\tau_{xy} = \frac{\sigma\sqrt{\pi a}}{\sqrt{2\pi r}}\left(sin\left(\frac{\vartheta}{2}\right)cos\left(\frac{\vartheta}{2}\right)cos\left(\frac{3\vartheta}{2}\right)\right). \quad (2.24)$$

From these equations, we can see that, at $r = 0$, the crack tip, all stresses tend to infinity and a re pr oducts of t he geometrical pos ition $\frac{1}{2\pi r}f(\theta)$ and a f actor $\sigma\sqrt{\pi a}$, which determines the magnitude of the elastic stresses at the crack tip field. This factor is called the Mode I SIF,

$$K_I = \sigma\sqrt{\pi a}. \quad (2.25)$$

This is Equation (2.2) and is repeated here for clarity purposes. It is worth noting that this SIF is only valid for infinite plate. The geometry for a finite-sized plate has an effect on crack tip stress field. Therefore, we can modify (2.25) by including a correction factor,

$$K_I = C\sigma\sqrt{\pi a}.f\left(\frac{a}{W}\right) \quad (2.26)$$

where C and $f\left(\frac{a}{W}\right)$ can be determined by stress analysis. Different geometries, SIF and geometric factors for different specimens have been obtained, (see work of [3,6]).

2.1.7 DETERMINATION OF K_I USING J-INTEGRAL METHOD

Consider a homogeneous body of linear or non-linear elastic material free of body forces [17]. Strain energy function W is defined by:

$$\mathbf{W} = \mathbf{W}(x,y) = \mathbf{W}(\epsilon) = \int_0^{\epsilon} \boldsymbol{\sigma}\, d\epsilon \tag{2.27}$$

where $\epsilon = \frac{1}{2}[\nabla \boldsymbol{u} + \nabla \boldsymbol{u}^T]$.

Now consider the J integral defined by:

$$J = \int_{\Gamma} \boldsymbol{W} d_y - \boldsymbol{t}.\frac{\partial \boldsymbol{u}}{\partial x} dx \tag{2.28}$$

where $\boldsymbol{t} = \boldsymbol{n}.\boldsymbol{\sigma}$ is the traction vector, $\boldsymbol{u}$ is the displacement vector and $\boldsymbol{n}$ is the normal to the chosen region surrounding a crack, see Fig. (2.5).

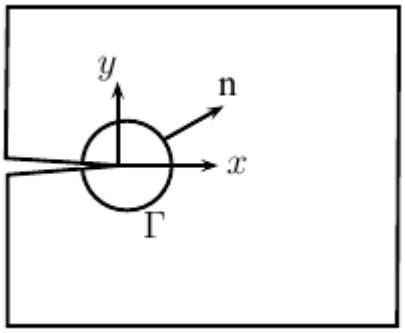

Figure 2.5. The integral is taken around the circle surrounding the crack tip. This region is denoted here as $\boldsymbol{\Gamma}$ and the normal to this ring in denoted as $\boldsymbol{n}$.

The *J*-Integral can also be written in index notation:

$$J_i = \lim_{\epsilon \to 0} \int_{\Gamma} \left(W_{n_i} - n_j \sigma_{jk} \frac{\partial u_k}{\partial x_i} \right) d\Gamma \tag{2.29}$$

where J_i is the component of the J-integral for crack opening in the x_i direction and ϵ is a small region around the crack tip. For isotropic, perfectly brittle, linear elastic materials, the J-integral can be directly related to the fracture toughness, which describes the ability of a material containing a crack to resist fracture. When representing purely elastic material, K_I will be related to the J-integral as follows:

$$K_I = \sqrt{JE'} \tag{2.30}$$

where K_I is the stress intensity factor, J is the J-integral and $E' = E$ for plane stress cases, and $E' = \frac{E}{1-v^2}$ (v is the poisons ratio) for plane strain.

It is worth noting at this point that Equations (2.28) and (2.30) were used to calculate the stress intensity factors and the Abaqus finite element code was used to evaluate the contour integral using the domain integral method [18]. Abaqus uses an interaction integral to measure the share of each mode in the energy release rate it calculates through a domain integral method, and the stress intensity factors can be computed using the following equation:

$$K_I = \left(\frac{8GJ}{1+\kappa}\right)^{\frac{1}{2}} \tag{2.31}$$

where $G = \frac{E}{2(1+v)}$ is the shear modulus and

$$\kappa = \begin{cases} \frac{3-v}{1+v} & \text{for plane stress} \\ 3-4v & \text{for plane stress.} \end{cases} \tag{2.32}$$

Abaqus produces SIF using the ring of contours surrounding a crack tip. The convergent value of any set of contours was taken to be the stress intensity value for that particular crack length. If, for example, the contours do not converge, an average value of contours can be taken and plotted against crack length. This is found to be valid, since the contour along the crack tip converges to the same value as we move further away from the crack tip. The way the SIF is evaluated in Abaqus will be discussed in more detail in Chapter 5.

2.1.8 FATIGUE CRACK GROWTH AND THE FATIGUE THRESHOLD

In the design of many engineering components subjected to cyclic or repetitive loading, fatigue is an ever-present challenge. Fatigue is a permanent structural change that occurs in a material subjected to repeated loading at stresses that have maximum values less than the static yield of the material.

In industry, the engineer often endeavours to design the structural or component system in such a way that the cyclic stresses are below a particular fatigue limit, or, in fracture mechanics terms, at stress levels below fatigue threshold. In the Paris formulation of fatigue, threshold ΔK_{th}, may be regarded as that value of cyclic stress intensity below which fatigue crack growth does not occur. It is also regarded as a function of material, the test conditions and the environment.

For a particular material and environment, this threshold value, ΔK_{th}, is determined experimentally by monitoring growth of a crack (typically in a compact tension (CT) specimen) and continually reducing cyclic stress levels until the threshold condition is reached [19, 20].

To apply this to problems of cyclic loading (fatigue), replace Equation (2.2) or (2.25) by:

$$\Delta K = Y\Delta\sigma\sqrt{\pi a} \tag{33}$$

where the stress amplitude, $\sigma = \Delta\sigma = \sigma_{max} - \sigma_{min}$ and the SIF, $K = \Delta K = K_{max} - K_{min}$. The dimensionless correction factor, Y, is introduced in the two equations and also in Equation (33) in order to characterize the geometry:

$$Y = f\left(\frac{a}{W}\right) = \frac{\left(2+\left(\frac{a}{W}\right)\right)\left[0.886+4.64\left(\frac{a}{W}\right)-13.32\left(\frac{a}{W}\right)^2+-\cdots\right]}{\left(1-\frac{a}{W}\right)^{\frac{3}{2}}}. \tag{2.34}$$

In this case, W is the width of the specimen or, more precisely, the width of the compact tension specimen.

Using the concept of stress intensity range, the life of a fatigue crack can be plotted on a graph of crack growth rate $\frac{da}{dN}$ vs. ΔK, the stress intensity range.

The life of an average crack is divided into three regions, which, for clarity purposes, will be called: Threshold region, Paris region and Fast fracture region, as shown in Fig. (2.6).

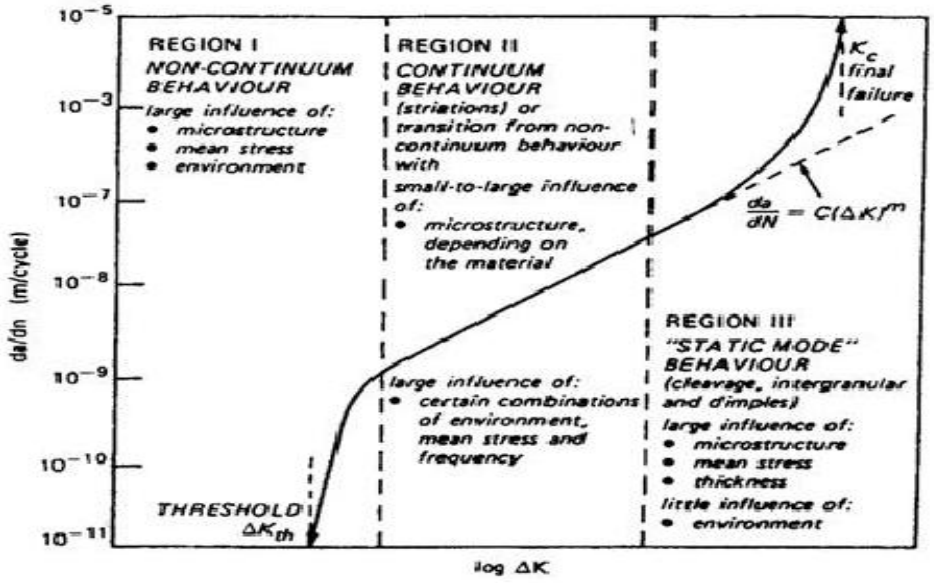

Figure 2.6. The Paris curve showing 3 different regions of the fatigue crack growth rate curve [1].

Our focus is in the first region, where the threshold value can be obtained. The threshold SIF, K_{th}, may also be related to the level at which the crack will stop or continue growing subject to the load stress. Below ∇K_{th}, the crack will stop growing, and, above threshold, the crack will continue growing. This is why it is important to know the threshold value for a particular material. There have been a number of methods proposed to determine this value. However, they are time-consuming and have limitations on the loading conditions.

Paris-Erdogan law relates the stress intensity factor range to sub-critical crack growth under a fatigue stress regime:

$$\frac{da}{dN} = C\ \Delta K^m \tag{2.35}$$

where da is the length which changes from the initial crack length to the critical crack length when fracture occurs, $da = a_c - a_i$, (where a_c is the critical crack length and a_i is the initial crack length.), N is the number of load cycles, C and m are the material constants, and ΔK is the range of the stress intensity factor.

This equation is of fundamental importance in a sense that fatigue life prediction can be found after integration. Using (2.33) and (2.35), we can derive the number of load cycles as follows:

$$\frac{da}{dN} = C\,\Delta K^m = C(\Delta\sigma Y\sqrt{\pi a})^m \tag{2.36}$$

which, when we integrate both sides, between initial flaw size to the final flaw size, we get:

$$N_f = \int_{N=0}^{N=N_f} = \int_{a_f}^{a_{crit}} \frac{da}{C(\Delta\sigma Y\sqrt{\pi a})^m}\,. \tag{2.37}$$

Hence, fatigue life prediction can be known. In most engineering applications, there are different factors affecting the structures. If more dependent variables are taken into account, this equation can prove to be difficult to integrate since the geometric factor depends on a, the crack length; hence we can rely on numerical methods for the solution process.

2.1.8.1 Methods of Determining fatigue life

There are different methods with different issues involved when determining the SIF threshold ΔK_{th} value. Analytical, experimental and computational methods will be

described, but the main focus will be on the computational part which forms part of this project.

2.1.8.1.1 Analytical Methods

As mentioned above in the previous section, the fatigue life prediction equation can prove difficult to apply, especially to industrial problems. However, a number of theories and engineering laws have been proposed to overcome the difficulties.

The simplest and one of the first methods used was the Palmgren-Minor rule, which is the most simple assumption to determine the fatigue lifetime under variable amplitude cyclic loading. It was first proposed by Palmgren (1924) and Minor (1945). This rule restricts the body to only tolerate a certain amount of damage, D. If the body experiences D_i $(i = 1, 2, \dots N)$ damages, from M number of sources, then the failure will occur if:

$$\sum_{i=1}^{M} \frac{D_i}{D} = 1 \tag{2.38}$$

where D_i/D is the fractional damage from the source. In FM terms, this rule relates data for $\frac{da}{dN}$ vs. ΔK via the Palmgren-Minor linear rule. This is similar to the discussion that we had earlier on fatigue life prediction. It ignores the effects of loading conditions, and hence the accuracy of the resulting fatigue life prediction is generally poor.

Elber (1971), introduced the plot of crack closure against effective SIF, K_{eff}, which is the difference between the maximum SIF, K_{max}, and SIF below which the crack remains closed, K_{op}, the effect of loading sequence and stress ratio disappear. Based on these, several models to calculate K_{eff} have been proposed. For example, in Newman (1992,

1995), the Dugdale-Barenblatt strip yield model was proposed, where K_{eff} was calculated analytically with the use of the stress level required to counteract the resistance exerted by the residual plastic deformation. The crack growth rate was found to be given by:

$$\frac{da}{dN} = C{K_{eff}}^m = C(K_{max} - K_{op})^m = C\left[\frac{(1-\sigma)/\sigma_{max}}{1-R}\right]^m \Delta K^m \quad (2.39)$$

where m and C are determined experimentally, σ is the applied stress, and R is the ratio $\frac{\sigma_{min}}{\sigma_{max}}$.

Ewald and Wanhill [1] also reported the other value to assist with life prediction to be calculated using fracture threshold value $\Delta K_{th} = E\,\epsilon_f\sqrt{2\pi\rho}$. In this case, E is the young modulus, ϵ_f is the fracture strain, and ρ represents the radius calculated experimentally to be equal to the fracture strain.

2.1.8.1.2 Experimental Methods

Frost and Dugdale [21] developed the early studies on fatigue threshold. They observed that, with non-propagating cracks, cracks developed at the notches. They also developed a relationship between the crack length and the stresses necessary for crack growth.

The sigmoidal shape of a crack growth ration da/dn data has been recorded, as shown previously in Fig. (2.6), to be in a region of 10^{-10}m/cycles for most materials. Paris et al. were the first to determine the threshold value, ΔK_{th},, at crack growth rates of the order of 2.5×10^{-11}m/cycles. This was obtained from situations where existing material flaws

were small and lightly stressed but subjected to a large number of cycles over their lifetime. It was then of interest to study slow fatigue crack growth where a compact test specimen was used. Pearson [22] was the first to document that cracks could grow at SIF levels below the threshold level. To determine the valid threshold values for a specific material, it is necessary to reduce gradually the applied SIF range.

In applications where initial defects are large, for example in welded civil engineering structures, the fatigue cracks are also large and, therefore, small cracks are not of much importance.

2.1.8.1.3 Computational Methods

Finite element methods and direct numerical simulations have been used to investigate fatigue life. The main focus here is in the Finite element method, and it will be discussed in detail in section (2.3).

2.2 Fracture Mechanics Specimens

In this project, we looked at the two fracture mechanics properties. The first property that we investigated was the fatigue threshold, which was then followed by the second property, the fracture toughness. These properties have their own different fracture mechanics specimens that we focus on. The former is the Compact Tension specimen that leads to develop the specimen (produce decreasing SIF) that is part of the focus of this project. The latter is the Double torsion specimen, which was also investigated, and our aim was to contribute to DT standardization in literature.

2.2.1 SPECIMEN USED FOR FATIGUE THRESHOLD

One of the standard specimens that is normally used in FM laboratory testing is the Compact Tension (CT) specimen, Fig. (2.7). CT has been used by many researchers in the laboratory, and both analytic and numerical studies have been documented [7,23,24,25,26]. It is well known for its easy SIF evaluation for any crack length a where the ratio a/W may be obtained, the corresponding value of Y which gives the geometry parameter, breadth B and load applied may be used to obtain the value of K_I. In a standard fatigue test, the SIF are determined by:

$$\Delta K = \frac{\Delta P.Y}{B\sqrt{W}} \tag{2.40}$$

where ΔP is the applied load, B is the specimen's breadth, and W is the width of the specimen. The specimen geometry is given previously in Equation (2.34).

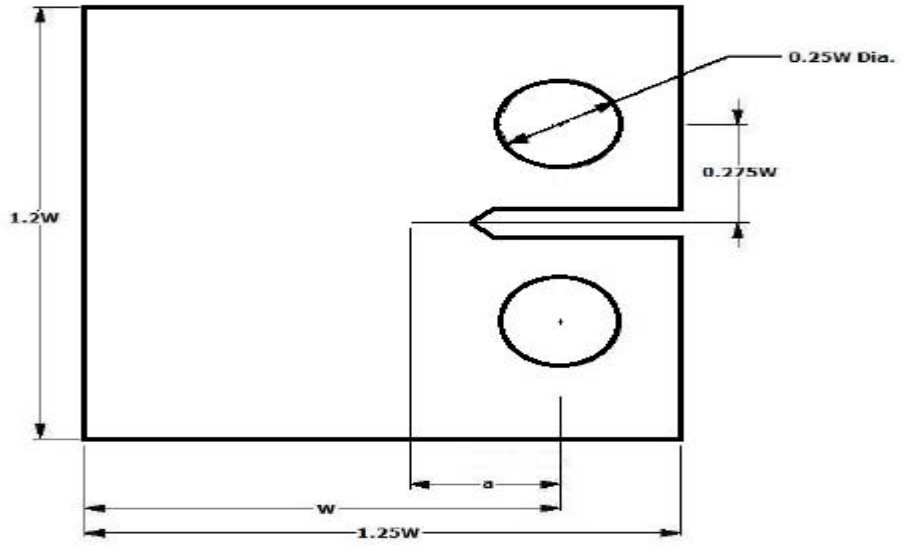

Figure 2.7. Compact Tension specimen showing geometry dimensions for the standard geometry model [11].

The CT specimen contains two open loading holes and a pre-included crack in between the holes. The force is applied through the two holes in opposite directions and adjusted until the crack starts to grow perpendicularly to the applied stress or loads, and the stress at the crack tip is then recorded. It is important to maintain a slow-growing crack in order to allow valid measurement of results to be recorded carefully and accurately.

This cannot be achieved if the crack grows faster. One of the reasons that contributes to fast crack growth is the material used, either brittle or ductile material. For brittle material, high/rapid crack growth is reached and the material may reach the point of failure before all FM properties are recorded. The plastic behaviour on ductile material may help to reduce the rapid crack growth, which in turn is overcome by the high forces owing to the testing setup resulting in an unstable crack growth. It is for these reasons that different tests are required for different materials. These are illustrated in Fig. (2.8).

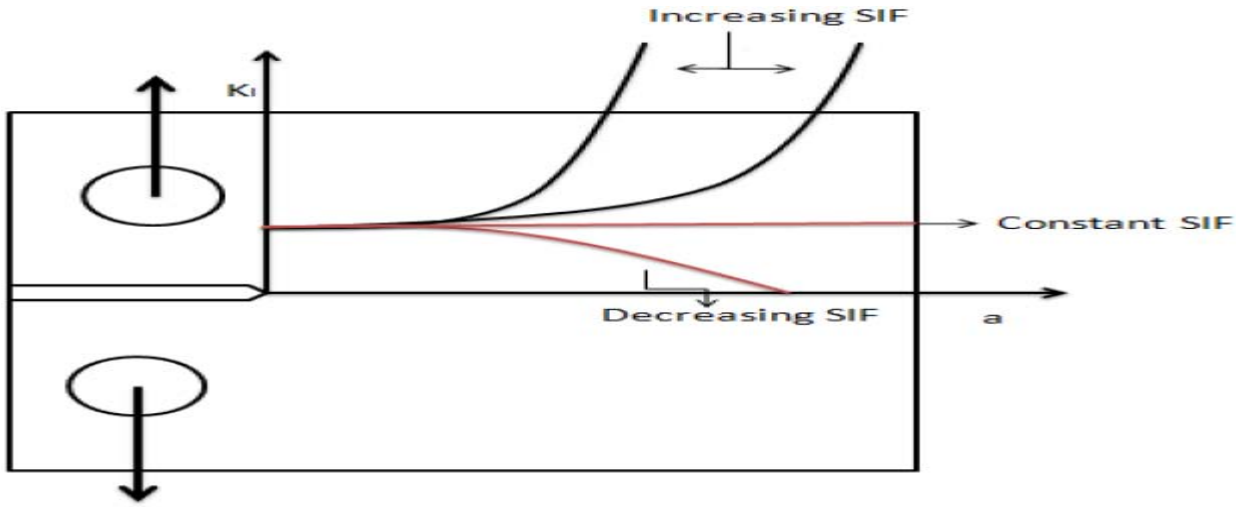

Figure 2.8. Schematic representation of different SIF curves obtained for different materials. The focus of this project is on the constant and decreasing SIF curves.

The two increasing curves represent the ductile material, where the crack grows fast, and the brittle material, which produces increasing SIF with crack length. Fast, rapid crack growth may be experienced in highly brittle material owing to no plasticity being present in the material. Ductile material may reduce the fast crack growth; however, owing to the specimen setup, fast crack growth may be experienced. When these materials are used during fatigue testing and the geometric dimensions and applied loads are applied, it is possible to obtain FM properties, and sometimes the results may be inaccurate.

Recent improvements have been made to overcome the CT geometry FM property measures. One of the geometries that have been proposed can be found in the work of Rosie et al. [7], where the breadth of the CT geometry was proposed to be left constant and the focus was given to the height. They proposed that the CT geometry might be adjusted along the region where the crack grows, and this might help to reduce stresses

and hence p roduce d ecreasing SIF w ith c rack l ength. Once the g eometry h ad been standardized, it would have a huge impact on the FM literature, since it would provide us with the new specimen which allows for the determination of the fatigue threshold value. It would help us to find the point of arrest in the material and hence find the threshold (discussed in more detail in Chapter 3).

2.2.2 SPECIMEN USED FOR FRACTURE TOUGHNESS

The D ouble T orsion (DT) geometry is a te st s pecimen c onfiguration t hat f acilitates fracture in vestigations in highly b rittle ma terials and is well known to p roduce a s tress intensity f actor t hat i s i ndependent of c rack l ength. T his f eature allows f or t he propagation of r elatively long c racks i n a hi ghly c ontrolled manner i n e xceptionally brittle materials.

A typical geometry consists of four point loads and the support at the far end. The crack propagates between the loads to the direction of the fixed end, see Fig. (2.9).

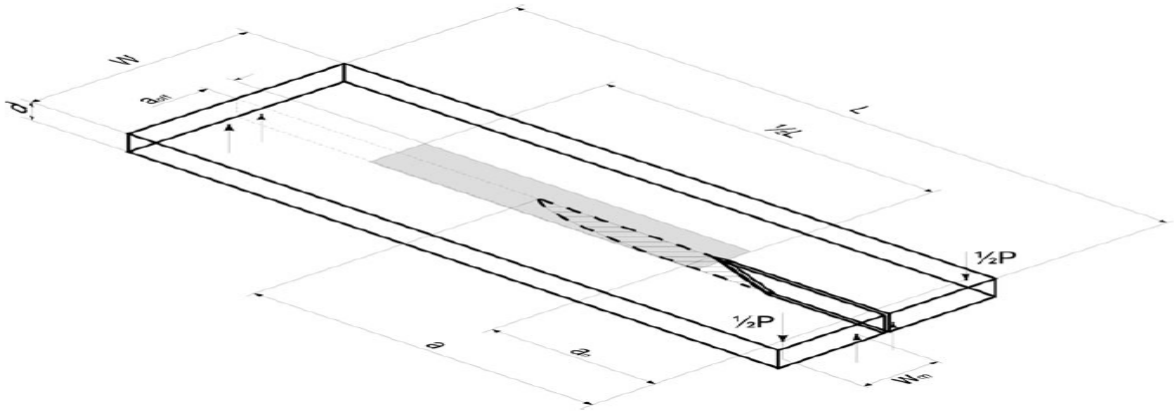

Figure 2.9. DT geometry illustration, it consists of dimensions and the load configuration [27,28].

To date, however, the DT geometry is yet to be standardised and many questions remain regarding optimal specimen dimension, load point deflections, and out-of-plane deformations. This project aims to investigate the DT geometry using the Finite Element Methodology [29] in order to obtain an optimum specimen geometry that can be utilised in fracture toughness and other fracture-mechanics-related investigations. More details, theory and modelling of DT geometry can be found in Chapter 5.

2.3 Finite Element Method

Numerical methods have been successfully used to study SIF and for modelling in FM over the years [30-38]. One of the methods mainly used for modelling is the finite element method (FEM). The basic idea behind FEM is to discretize the domain into elements in which one element can be analysed at a time. The elements can either be bricks or triangles [30]. In this project, we look at the two finite element methods that have been used, the conventional finite element method and the extended finite element method, to analyse the fracture behaviour of the Compact Tension (CT) specimen and the decreasing tapered double cantilever beam (DTDCB). The DT specimen will be analysed using only the conventional finite element method.

The FEM method can be briefly summarised as follows:

Begin by setting out the strong form, which is the equilibrium equation that describes the physical model of the body. This is followed by the weak form, which is the reduced higher derivative of a strong form after integration. The solution can then be easily found by solving the final matrix equation. During the solution process of the weak form, it is

required to find the space functions, $\boldsymbol{u}$, which will be used as solution approximations of the equations. These space functions are approximated using conversional FEM and the extended FEM in this project.

2.3.1 CONVENTIONAL FINITE ELEMENT METHOD (CFEM)

The basic idea in the CFEM method is to capture the singularity in the crack front region. The introduction of the stress tip singularity was performed earlier by Tracey [30]. The generalized stress tip singularity can be expressed as r^{-p}, where r is the radial distance from node 1,8,7 (from Fig. (2.12)), triangular element.

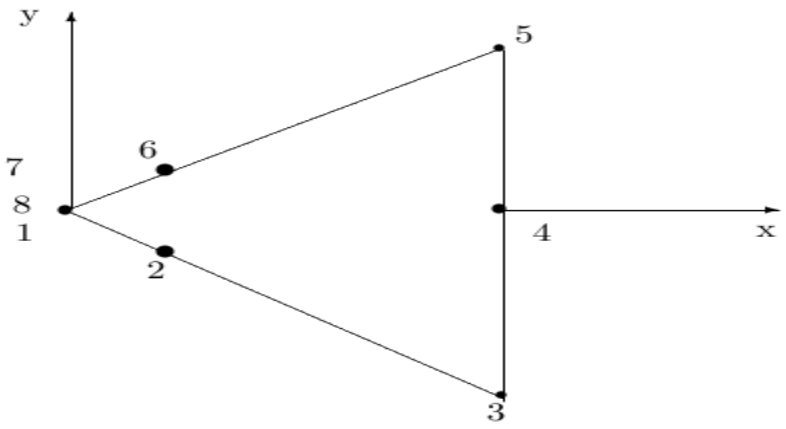

Figure 2.10: Collapsed 8-node element. Nodes 1, 7 and 8 are combined to a single node, while nodes 2 and 6 are shifted closer to the combined node.

The elements that can model such singularity are the cubic (3D) elements called wedges. These elements were applied to the DT specimen since its crack length is inclined. It is worth mentioning that such elements were not necessarily used in the CT and DTDCB

specimen, as the crack is perpendicular to the horizontal and the mesh does not introduce angles that would introduce difficulties in the solution process.

2.3.2 EXTENDED FINITE ELEMENT METHOD (XFEM)

The Extended Finite Element Method (XFEM) has been used for almost a decade, heading back to its beginning when it was first implemented by Belytchko and Black [35]. They modeled a crack using XFEM. The basic idea of XFEM is to model the discontinuities based on the partition unity method [31,32,33] and that the crack does not have to conform/be in-line with the mesh generated [34].

The XFEM is basically a method of modelling discontinuities in geometries. XFEM is used to model crack initiation and propagation along an arbitrary domain, without a need to re-mesh the model [10]. This is the most crucial aspect of applying the finite element model. XFEM is advantageous in the sense that it will determine the point at which the propagation has stopped growing. It differs from the previous method where the crack is extended even if the geometry and the properties of the material, in real life, do not allow such propagation.

2.4 Conclusion

The basic aspects of fracture mechanics have been summarised in this chapter. Without this basic understanding, the numerical implementation, FEM would be difficult to understand properly. This chapter described the basic idea of fracture mechanics, which

was then followed by the fracture mechanics specimens relevant to this thesis, and the modelling approach was also described. The basic background of the specimens provided here should be the basic background for the reader to understand the relationship between fracture mechanics and the specimens used. In the following chapter, a summary of previous related studies will be given.

CHAPTER THREE

THEORY OF EXPERIMENTAL STRESS INTENSITY FACTOR MEASURES

This chapter aims to describe how the aims of this project will be reached. Firstly, the approach used to answer the decreasing SIF (to achieve fatigue threshold) is described, where the basic specimen theory is given in detail. Secondly, the second aim is given in detail, which helps to achieve the second goal of using the DT specimen (allowing for brittle material investigation).

To begin this section, it is important to state that the decreasing SIF specimen is based on the compact tension specimen. It is for this reason that this chapter will begin by looking at the compact tension specimen in detail, where SIF are derived, and this will be followed by the decreasing SIF specimen (DTDCB). The DTDCB specimen derivation will also be given.

The Double Torsion geometry will be described in detail. This includes the relevant literature review and the SIF derivation of the geometry.

3.1 Compact Tension Specimen Theory

The compact tension (CT) specimen has been successfully studied by many authors over the years; for example, numerically [39-42] and in the laboratory [26, 43]. Investigations have been in both the energy and SIF approach. Prowoto et al. have recently successfully performed two-dimensional [44] and three-dimensional [39] modelling to compute the plastic zone in front of a crack in the CT specimen. The model that they developed

focuses on the effect of microstructural morphology in multiphase steel in three dimensions utilizing commercial software. This had a huge impact in the FM field, since it focused on the microscopic parts of the FM specimens. This had not been possible before owing to computational limitations. Nonetheless, there are still many CT aspects that still need to be investigated. For example, CT specimen is understood to produce increasing SIFs. Decreasing SIF specimen that will produce the threshold fatigue values and is based on CT, is still needed.

Rosie et al [7] investigated, experimentally, the influence of increasing the breadth of the CT specimen, as shown in Fig. (3.1). The aim of developing such a specimen was to increase the area in such a way that the part where the crack grew would reduce the stresses and hence the SIFs. This specimen proved to be problematic to implement, as it caused failure at the loading holes owing to high stresses that were concentrated when high loads were applied. This resulted in a need to investigate other geometries.

In this work, we expand the work by Rosie et al. and investigate the increase in height of the specimen when the breadth is kept constant. The hypothesis behind this investigation is that the cross-sectional area, along the breadth, where the crack is propagating, does not change, except in the direction that the force is applied. This area opposes the force, hence it reduces stresses along the crack propagation direction and SIFs will eventually decrease.

Having this in mind, it is worth mentioning that the specimen parameter that we looked at during the specimen development is the height. We began with the CT specimen and increased the height from a small distance measured from the loading points. Then the CT specimen was used as a reference to validate the FEM methods. The basic idea was to

apply the method to the model and compare the results obtained with the literature for verification. As such, if the results were in agreement with the literature, then it would be assumed that the method was valid and could be applied to extended models or geometries of the CT specimen.

3.1.1 DERIVATION OF SIF USING CT SPECIMEN

We saw in Chapter 2 that the SIF was related to the energy release rate G according to the following relation:

$$G = \frac{K_I^2}{E} \quad \text{plane stress} \tag{3.1}$$

$$G = \frac{K_I^2}{E}(1 - v^2) \quad \text{plane strain} \tag{3.2}$$

where v is the poison's ratio and E is the young modulus. We can follow the same energy approach as in Chapter 2, Section 2.1.4. The only difference is that, at this time, we were using the CT specimen shown in Fig. (2.7), Chapter 2. This analysis was given early on by Irwin [45], and the complete derivation can be found in [1].

In addition, the development of CT SIF was based on the following assumptions:

- The direction of maximum principal stress is in the direction of applied load. Therefore, the crack is propagated in the direction perpendicular to the loads.
- The initial SIF at the notch tip is sufficient to ensure a fatigue crack will propagate.

- The material is homogeneous.
- The strains are small (no large displacements).
- The crack profile remains constant.
- The displacements are small everywhere, so that their squares may be neglected.
- The rupture occurs in a tensile test at stresses corresponding with maximum resultant pull [4].

If we consider the body in Fig. (2.7), loaded by force P, it has been shown [1] that the energy release rate is governed by the following equation:

$$G = \frac{d}{da}(F - U_a) \tag{3.3}$$

where F is the external force, a the crack length, and U_a is the elastic strain energy.

Or, when accounting for external work done by the force per unit length, i.e. $F = Py$ and the change in elastic strain energy release caused by the introduction of a crack in the body is given by $\frac{Py}{2}$, we obtain:

$$G = \frac{1}{B}\left(P\frac{dy}{da} - \frac{dU_a}{da}\right) = \frac{1}{B}\left(P\frac{dy}{da} - \frac{1}{2}\frac{dPy}{da}\right) \tag{3.4}$$

where B is the specimen thickness which is introduced to account for specimen thickness, which is constant in this case, and y is the displacement at the load. The inverse of the body's stiffness is called the compliance, C, which is the ratio of the load displacement and the force applied to the body, $C = \frac{y}{P}$. If we substitute the compliance relation to Equation (3.4) we get:

$$G = \frac{1}{B}\left(P\frac{dCP}{da} - \frac{1}{2}\frac{dCP^2}{da}\right) \tag{3.5}$$

and applying chain rule:

$$G = \frac{P^2}{2B}\frac{dC}{da}. \tag{3.6}$$

For constant P, we can relate the energy release rate to SIF as follows:

$$K_I = \sqrt{E'G} = P\sqrt{\frac{E}{2}\frac{dC}{da}} \tag{3.7}$$

or

$$K_I = \sqrt{E'G} = P\sqrt{\frac{E}{2(1-\nu^2)B}\frac{dC}{da}}, \tag{3.8}$$

where E' accounts for the plane stress (Equation 3.7) or plane strain (Equation 3.8). These equations provide a useful approach to the development of the new specimen that will result in decreasing SIFs by allowing certain parameters on the left-hand side of Equation (3.8) to decrease. For example, we can keep all the parameters on the right-hand side constant except dC/da, which will be made to decrease. This is discussed in the development of the decreasing SIF section below.

3.2 Development of Decreasing SIF specimen

This specimen was developed using a Decreasing SIF Tapered Double Cantilever Beam (DTDCB) specimen which had been used in the literature before [1]. It is well known that if the crack length is varied with the height of the Tapered Double Cantilever Beam (TDCB) specimen so that the relation between the two is kept constant, the resulting SIF will remain constant, according to the following equation:

$$C = \frac{8}{EB}\left(\frac{a^3}{h^3} + \frac{a}{h}\right) \tag{3.9}$$

where a is the crack length, h is the tapered height, and C is a compliance constant. The SIF is related to C according to the following equation (modification of Equation (3.8) to account for grooves, if present):

$$K_I = P\sqrt{\left(\frac{E}{2B_n(1-\nu^2)}\frac{dC}{da}\right)} \tag{3.10}$$

where

$$\frac{dC}{da} = \frac{8}{EB}\left(\frac{3a^2+h^2}{h^3}\right) \tag{3.11}$$

is the constant term when a and h are varied, so that the term inside is constant and B_n is the side grooves, while B is used if no grooves are present. Further details can be obtained in the work of Deshayes et al. [46].

The TDCB specimen can be extended to satisfy the goal of our project as follows:

If the height, h, is increased to a point where $\frac{dC}{da}$ is decreasing along increasing crack length, i.e., the denominator increases at the power of three, then we expect this term to decrease as well. These results were used to develop the new decreasing tapered double cantilever beam (DTDCB) specimen. The first specimen dimension profile that was used by Rosie et al. [7] is shown in Fig. (3.1). This investigation was based on the case where $B = B(a)$ which failed at the loading holes, owing to high stresses needed to propagate the crack, see [7]. Hence, new specimen geometry needed to be proposed. However, Deshayes et al. [46] had already studied such a specimen. Therefore, in this project, the focus was to study such a specimen in more detail.

In this case, using equation (3.9), the goal is to keep the compliance C constant. This is done by keeping the breadth constant, increasing the crack length and choosing height h which will always produce constant C. Then Fig. (3.2) was produced with the following dimensions:

$L = 215.9mm$, $B = 24.2mm$, total height $h = 152.4mm$ and $\theta = 73.3^{\circ}$,
where θ is the height inclined angle.

These dimensions were analysed and it was found that they satisfy Equations (2.1) and (3.9). The plotting of a against h, keeping C constant, results in the specimen in Fig. (3.2). This is done by keeping C constant and choosing a crack length value from the loading hole, so that the height h can be obtained. The resulting, and most suitable, geometry of the modified CT specimen is found after modelling different specimen configurations and will be presented in the results section, Chapter 6. The geometries will be modelled in Abaqus, similar to CT specimen, as described in detail in Appendix A.

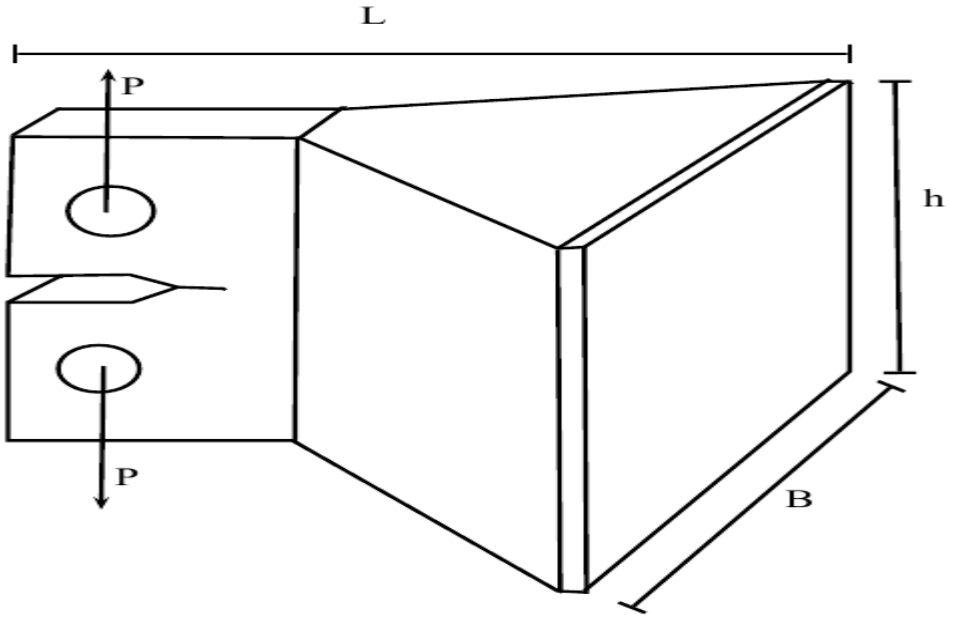

Figure 3.1. Increase in breath of the compact tension specimen. The breadth B depends on crack length, i.e. $B = B(a)$.

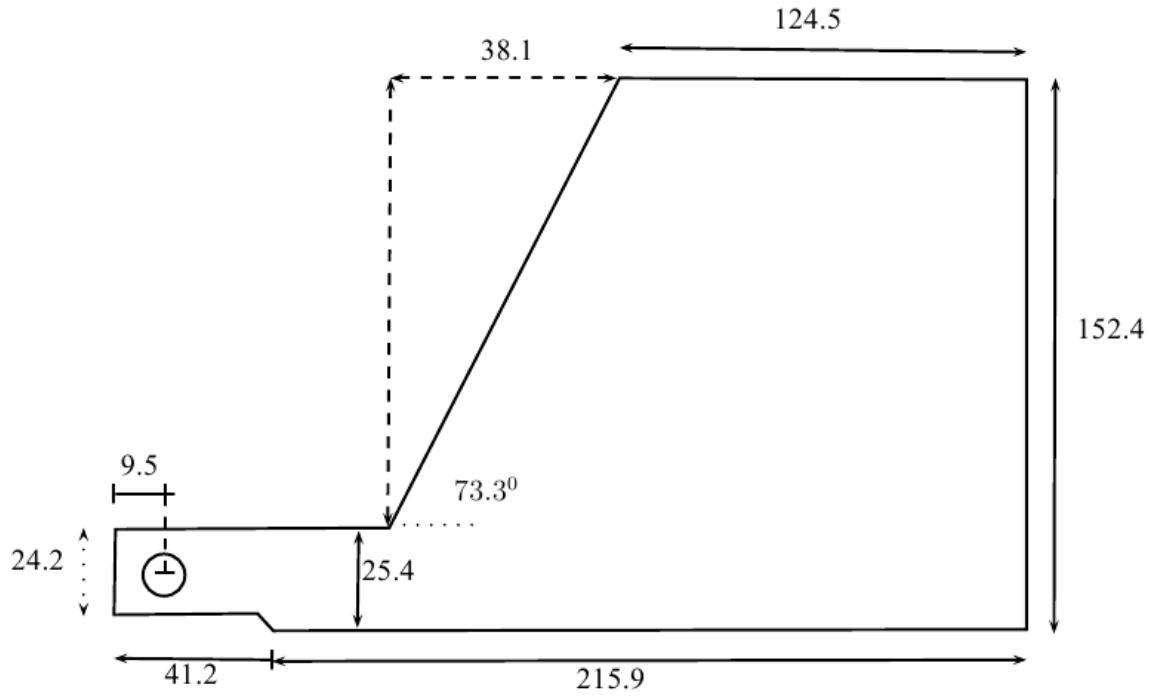

Figure 3.2. Resulting symmetric specimen geometry after CT specimen has been modified. The breadth, $B = 8mm$, is kept constant, while the height is crack length dependent, $h = h(a)$ and the units are in mm [46].

3.3 Double Torsion Geometry

The Double Torsion (DT) geometry, Fig (2.9), is a test specimen configuration that facilitates fracture investigations in highly brittle materials. The novelty of the DT technique lies in the property of a constant SIF regime during crack propagation [48], which is considered to produce a crack length independent geometry by achieving a constant stress intensity factor (SIF) regime [48]. As such, the DT geometry is commonly

used when testing highly brittle materials such as rocks [49], glass and ceramics [50] and nuclear graphite [51] for example. Furthermore, the technique is practical for situations where crack length measurements are not always possible (such as in high temperature test conditions) owing to the fact that the SIF is crack length independent and no crack length measurements are required during testing [48].

To date, however, several questions remain regarding the technique. The crack length independent SIF is not completely undisputed within the fracture mechanics community, as deviations from the crack length independent SIF have been observed [52-56].

The development of the DT technique is credited to the work undertaken by Outwater and Gerry (1969) [57], Kies and Clark (1969) [58] and William and Evans (1973)[59]. The load is applied in a four-point bend configuration at the one end (as shown in Fig. (2.9)), where the crack propagates through the centre of the specimen. The loading configuration is such that each specimen half, separated by the crack, is loaded in torsion. It is assumed that the compliance of the specimen is linearly dependent on the length of each torsion bar (i.e. the crack length) and that the unbroken ligament remains rigid during loading [28]. This assumption, however, has been found to have implications for the crack length independent SIF; the deformation of the un-cracked ligament has been shown not to remain rigid [28] and large deflections at the load point result in a non-linear torsional compliance (Leevers et al. [60]).

Several attempts have been formulated to model the geometry using the Finite Element (FE) method. Examples include Trantina et al. [61], who investigated the DT geometry using a three-dimensional finite element model. An agreement was found between numerically and analytically obtained SIF over the middle of the specimen, $0.18 <$

$a/L < 0.78$ (for a specimen geometry $W = 3$). The work of Ciccotti et al. [62,63] formulated a series of correction factors for a range of specimen geometry configurations to correct the deviations to the analytical solution.

Furthermore, Attia (2010) [48] performed a three-dimensional FE analysis, evaluating for the optimum thickness of the DT geometry, and observed deviations between the FE model and experimental data. The deviations have been attributed to the curvilinear crack front, which is typically modelled as a straight crack front in the FE environment. These studies have however not investigated an overall optimum specimen geometry ratio that allows for a crack-length-independent geometry. Presented in this project is the optimisation of the DT geometry, which provides a crack-length-independent geometry. It is the aim to contribute to the understanding of the DT geometry and the use of this novel test configuration. These were achieved by understanding the theory behind the DT geometry and modelled using FEM.

3.3.1 SIF OF THE DOUBLE TORSION GEOMETRY

In the DT method, the main assumptions of calculating the stress intensity factors (SIF) to determine the fracture toughness are:

- The loading is applied independently to each of the two halves of the specimen inducing small torsional deformations.
- The un-cracked portion of the specimen remains rigid.
- Linear Elastic Fracture Mechanics (LEFM) is assumed to be Mode I.

Based on these assumptions, it is possible to apply the solution of non-circular bars torsion to the DT beam (Fig. (2.9)).

This project follows the theoretical approach where the DT specimen is used to study the SIF. If we consider a bar with polar moment of inertia I_p and shear modulus μ subjected to a torsion moment T resulting in an angle of twist ɵ, the following relationship can be obtained:

$$\theta = \frac{y}{W_m} = \frac{Ta}{I_p \mu} \tag{3.12}$$

where y is deflection at the loads and a is the crack length.

The torsion moment T is given by:

$$T = \frac{P}{2} W_m \tag{3.13}$$

and the second moment of area for small twist angles is given by:

$$I_p = \frac{Wd^3}{6} \tag{3.14}$$

where W_m, the moment arm, is the distance between the two loads, p is the load, W is the width and d is the thickness. The relating of these three equations leads to a linear compliance which is obtained by assuming that the unbroken ligament remains rigid and only the cracked ligaments deform under torsion [52]

$$C(a) = \frac{y}{P} = \left(\frac{3w_m^2}{Wd^3\mu}\right)a \tag{3.15}$$

where y is the deflection caused by load P, w_m is the moment arm, d is the specimen thickness, W is the specimen width, and μ is the shear modulus.

The strain energy release rate G is related to the derivative of compliance (Mode I), assuming the crack extension area remains constant during crack propagation i.e., $dA = d \cdot da$. This leads to:

$$G = -\left(\frac{dU}{dA}\right) = \frac{P^2}{2d}\frac{dC}{da} \tag{3.16}$$

where, U denotes the total strain energy release rate. According to Williams and Evans (1973) [59], the relationship between the SIF (Mode I) and the energy release rate is given by:

$$K_I = \sqrt{EG} = PW_m\sqrt{\frac{3(1+v)}{Wd^4\Psi(d,W)}} \tag{3.17}$$

where Ψ is a thickness correction factor given by:

$$\Psi(\tau) = 1 - 0.6302\tau + 1.20\tau e^{-\frac{\pi}{\tau}} \tag{3.18}$$

and $\tau(d,W) = 2d/W$ [48].

As aforementioned, the crack front profile in the DT geometry is curvilinear. A crack front inclination is approximated by $c = \Delta a/d$, where Δa is the crack extension difference between the upper and lower surface of the test specimen [28]. Furthermore,

note that the SIF (in Eq. 3.17) is independent of crack length. It is this feature that allows for stable crack propagation in brittle materials.

3.4 J Integral

The j integral that is obtained in Abaqus may be used to approximate stress intensity which follows from equation (2.30). Abaqus uses elements surrounding the crack tip, or those that are specified by the user around the crack tip, to evaluate the contour integrals automatically. The user chooses the number of contours to be evaluated, and Abaqus evaluates the next ring of elements based on the previous ring until all chosen rings are evaluated [7]. In order to check solution accuracy, based on the number of element rings and the element formulation, the solution converges as we move far away from the crack tip. From this, a plot of contours from each crack length may be obtained, see the results section (Figure (5.2) for example).

In the literature, Rice [17] was the first to evaluate the j integral method. In this work, the j integral was applied to nonlinear materials to analyse the deformation of plasticity. Rice and Rosengren (1968) studied nonlinear materials and showed that the j integral may be used to characterise stresses at the crack tip. Linear and nonlinear models were investigated by Venkatachalam et al. [64]. They found that there was a change in a value of j integral when the load crosses elastic limits.

In this project, the j integral was chosen over the displacement extrapolation method based on the work of Courtin et al [65] for investigations in linear materials. They compared both displacement extrapolation and j integral, and they found that both methods performed reasonably well compared to the results of equation (2.40). When

both methods were tested in Abaqus, the j integral method was found to have an advantage over displacement extrapolation. This was found to be owing to the path integral evaluation which can be evaluated far from the singularities at the crack tip.

The SIF will be evaluated using the j integral in this project. CT and DTDCB crack front is perpendicular to the horizontal section of the model; hence, collapsing of elements is not necessary. To ensure accuracy, the crack front, which is the region of interest, will be modelled with a concentrated mesh surrounding the crack tip, and the other parts of the models can be meshed with scattered elements. On the other hand, since the DT model crack front is inclined, the use of a concentrated mesh will result in element angles that are much smaller than the required limit [7] and this may cause errors in Abaqus processing. Hence, collapsed elements will be used instead of concentrated mesh at the crack tip.

3.5 Conclusion

In this chapter, a summary was presented of the previous studies of geometries. The literature presented here, acts as the guideline and makes it possible to measure SIF of the corresponding geometries in order to measure the accuracy of the results in the present study. The critical aspect that was considered was the SIF for each model.

We first described the theoretical background of the CT specimen, and the SIF details were provided. This was then followed by the development of the DTDCB specimen, where the corresponding SIF was also presented.

The last section looked at the relevant literature review of the DT model. The corresponding SIF details were also provided.

From this chapter, we can now be able to apply the numerical methods, FEM, to investigate the geometries further. The implementation of FEM is given in the next chapter.

CHAPTER FOUR

METHODOLOGY

This chapter describes the modelling approach methodology that was followed in this project, the finite element method. In order to verify that the model approach would be valid, the known and widely used compact tension specimen was modelled first and the results were compared with the literature. Details of results can be found in Chapter 5.

Three geometrical models were analysed. The first section deals with the two models CT and the DTDCB, and the second section deals with the DT specimen. In addition, the CT and the DTDCB specimens were analysed using the XFEM method in order to obtain the point of no crack growth, and that point may be referred to as a SIF threshold value. It was not necessary to model the DT geometry in XFEM, since this is a well-known constant SIF model.

The CT and the DTDCB specimens were modelled using Abaqus version 6.10. The detailed implementation is given in Appendix A (CT and DTDCB geometries) and Appendix B (DT geometry)

4.1 CT and DTDCB Specimen

Both specimens had the same material properties, and they are both listed in the table below.

	CT	DTDCB
Young Modulus	207GPa	207GPa
Poisson's Ratio	0.33	0.33
Density	7860kg/m^3	7860kg/m^3
b	8mm	8mm

Table 4.1. Material properties for both CT and DTDCB specimens.

4.1.1 CONVENTIONAL FINITE ELEMENT (CFEM) MODEL

In Abaqus the model was created to be similar to the one that was created by Rosie et al. [26]. Note that during the model creation, the CT specimen and the DTDCB specimen models had the same mechanical properties but only different lengths, since the same material was used. Abaqus created a part as the defined specimen. The loading pin was modelled as the one that was an analytical rigid part, i.e. the deformation did not form part of the analysis and was modelled in the reference pin [7].

The assembly section was used to link the two parts, CT or DTDCB parts, with the loading pin. Both of these models were treated as independent parts. This was to allow us to have a simple and a clear meshing part to the specimens, except for the loading pin, which does not form part of the model. After the model was assembled, the mesh was created in order to form a partition. Linear hexahedral elements were used to mesh the whole specimen, and the resulting models are shown in Fig. (4.1) and (4.2). A total number of 62 796 elements were applied in CT and 24 072 in DTDCB specimen.

A degree of refinement was required around the area of concern, the crack tip region. As aforementioned, the elements at the crack tip had to be brick-shaped and concentrated. Abaqus allows an accuracy check to see where elements were too distorted for computational purposes.

In order to ensure convergence, a total number of 15 contours were chosen as the rings surrounding the crack tip. Close to the crack tip, at least three contours are required. The contours may not converge, therefore, the solution can be taken far away from the crack tip and this is one of the advantages of using j integral in Abaqus [7].

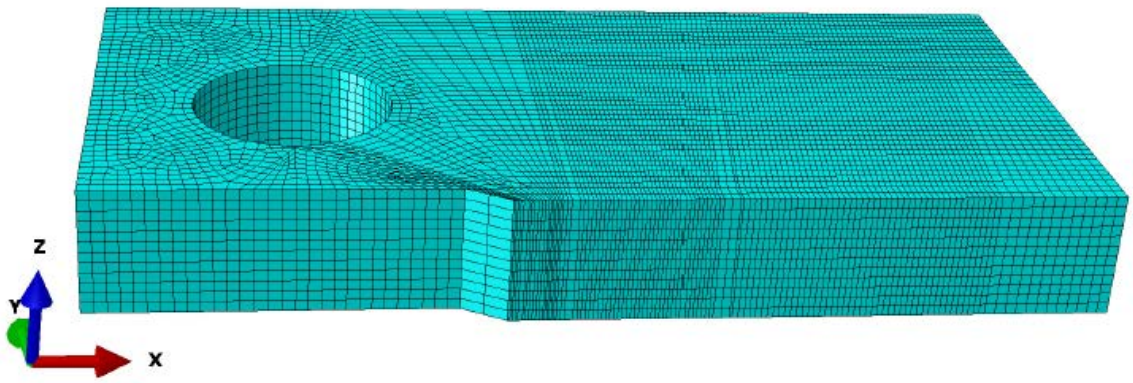

Figure 4.1. CT specimen showing the 8 node brick element mesh. The load was modeled as the rigid body with the surface-to-surface contact. RP is the point where the loads are applied.

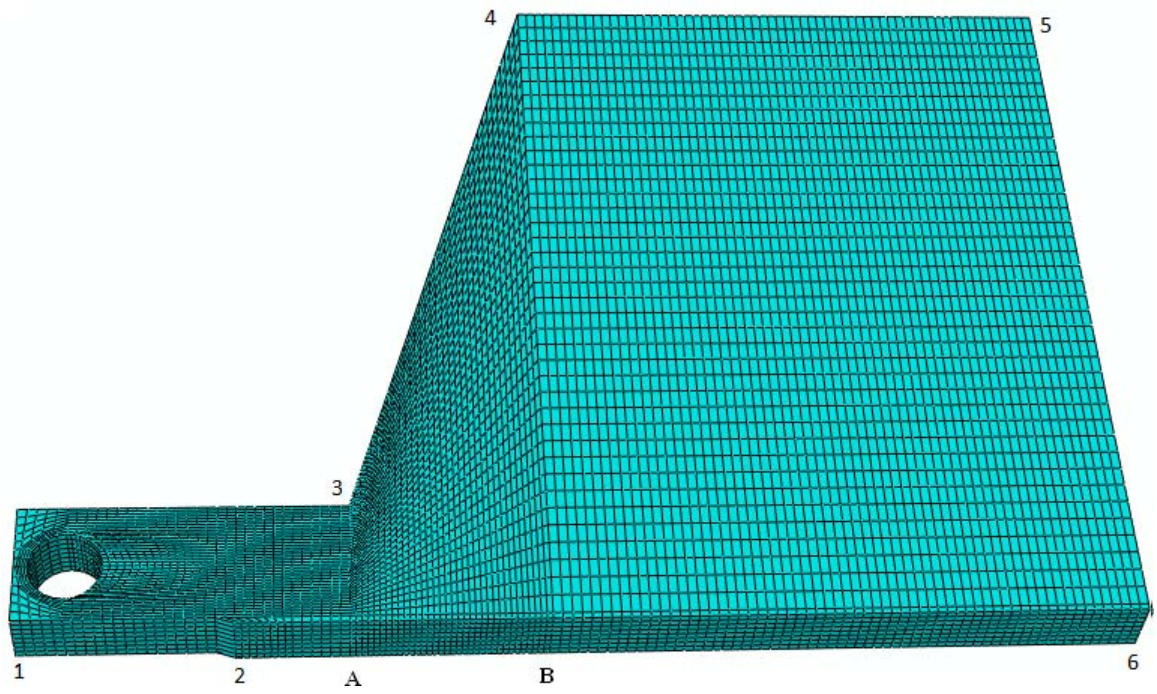

Figure 4.2. DTDCB specimen mesh geometry. The points of interest are points **A** and **B** where SIF are expected to decrease between the points.

During crack propagation, the two halves of the specimen interact. The interaction between crack surfaces was defined as a hard contact, and the Coulomb friction law for rough surfaces was applied, with friction coefficient of 0.5 [66]. The crack front was selected, and the direction was set to q-vectors as the direction where the crack would propagate. This direction is perpendicular to the load applied to a specimen [7].

A load of 7kN was applied to the CT specimen and the load of 11kN was applied to the DTDCB specimen. The symmetric boundary condition was applied to the y-direction, starting at the crack tip. We fixed the z-direction so that the specimen did not move

sideways, and the pin boundary condition was applied so that the pin was allowed to move in the y-direction only. The axis of both specimens is shown in Fig (4.1).

4.1.2 XFEM MODEL

The XFEM method makes modelling of propagating cracks easier and accurate since the mesh does not have to conform to the mesh. It allows cracks to be modelled independently of the mesh and allows the propagation of cracks without a need for remeshing. It also supports evaluation contour integrals of stationary cracks.
Since the XFEM is still new, it has some limitations in Abaqus. For example, only linear continuum elements can be used, only single or non-interacting cracks can be modelled, and a crack is not allowed to turn more than 90^{o}. For stationary cracks, the crack tip is located at any place in the domain, and for propagating cracks, the crack tip only cuts an element edge. Therefore, the crack can only arrest at an edge of an element, since it cuts an element completely. Hence, it is important to mesh the model with a high number of elements.

4.2 Double Torsion Specimen

Material properties for DT specimen are summarised in Table 2, and the sketch can be found in Fig. (2.9).

	DT
Young Modulus	3.7GPa
Poisson's Ratio	0.3
Density	$1.18 g/cm^3$

Table 4.2. DT material properties.

4.2.1 FINITE ELEMENT MODEL

As aforementioned, there have been a number of factors concerning the standardisation of the DT geometry test method. Some of these factors include the geometry aspects such as the specimen dimensions, specimen grooves, pre-cracking of specimen and deflection at the loadings, all of which still raise concerns and need to be investigated. This project, rather, focuses on the specimen dimensions.

To date, there have been a number of different recommendations made about the dimensions of the DT geometry. Most of these have been achieved with the use of the Finite Element models. For example, Trantina [67] utilised a FEM model where a specimen geometry of 0.1W thickness was used, and Ciccotti et al (55,62,63) used a thickness of 0.117 W in their FEM. The conclusions reflected on the use of large specimens so that large discrepancies between theoretical analysis and FEM analysis were found. Recommendations by Madjoubi et al [68] suggested that Evans' model can be used uncorrected for specimen lengths more than 3W and thickness of 0.075 [6].

Tait et al [69] suggested specimen geometries that could be used for DT testing. Those geometries were as follows (L:W:d) [6]:

- $3W{:}\,W{:}\,0.083W$ – PMMA
- $3W{:}\,W{:}\,0.120 - 0.10W$ – Polymer
- $2W{:}\,W{:}\,0.067W$ - Rock

Based on these observations, the DT geometry was also analysed using ABAQUS version 6.10, and the literature conclusions above were applied to this project to obtain optimum specimen geometry. In order to obtain the required optimum specimen geometry, nine geometry configurations were considered. These included three different length-to-width ratios (*L/W = 2, 3* and 4) and three different thicknesses-to-width ratios (*d/W = 0.06, 0.08* and 0.1), where $W = 50$ mm. Each test geometry was analysed at five different crack length ratios (*a/L = 0.25, 0.38, 0.5, 0.62, 0.75*) generating 45 models in total, see Table (4.3).

$\boldsymbol{d}(mm)$	$\boldsymbol{L}(mm)$	$a_1\,(mm)$	$a_2(mm)$	$a_3\,(mm)$	$a_4\,(mm)$	$a_5\,(mm)$
3	100	25	37.5	56	62.5	75
	150	37.5	56.25	75	93.75	112.5
	200	50	75	100	125	150
4	100	25	37.5	56	62.5	75
	150	37.5	56.25	75	93.75	112.5
	200	50	75	100	125	150
5	100	25	37.5	56	62.5	75
	150	37.5	56.25	75	93.75	112.5
	200	50	75	100	125	150

Table 4.3. 45 DT models.

4.2.2 MESH

Each model simulated the entire DT geometry, obtaining an average number of 6 047 quadratic hexahedral elements (Fig. 4.3). The mesh was refined near the crack tip using a concentrated mesh with collapsed elements, as illustrated along a vertical, long-axis cross-section in Fig. (4.4). This allowed for a better description of the strain field near the crack tip and has been validated against analytical solutions [61]. Numerical solution values of the associated SIF were calculated using the contour integral method. The computed *J*-integral was converted to an equivalent SIF using Equation (3.17), where *J*-integral was equivalent to *G*, from Equation (2.30). A convergence study followed similar to the previous methods. The contours surrounding the crack tip convergence was used to validate that the solution had been reached.

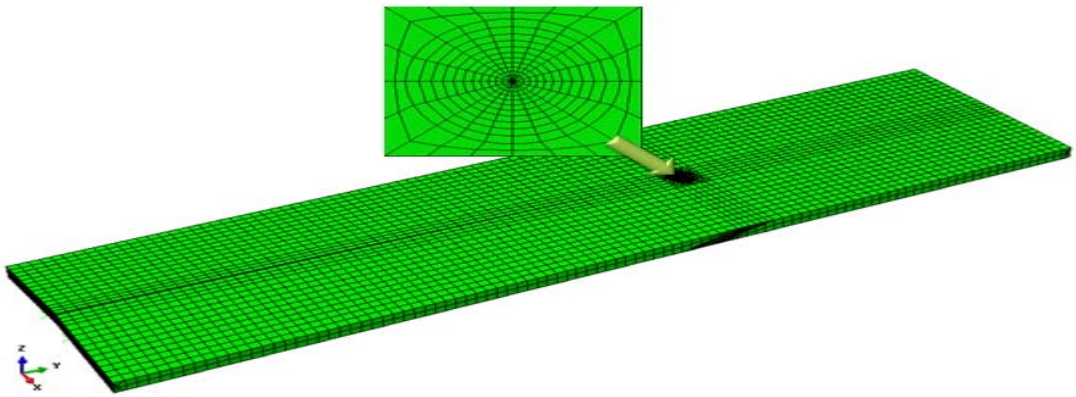

Figure 4.3. DT specimen meshed with quadrilateral hexahedral elements. A zoomed area around the crack tip showing a ring of element is also shown. Included is also specimen axis, x-axis the width, y-axis the length, and z-axis the thickness of the specimen.

4.2.3 BOUNDARY CONDITIONS

The boundary conditions of the model assumed that the nodes near the loading points (at the crack opening) were constrained in the y direction (front side - the side with the crack opening) and at the far side (the side at the back of the specimen) in the x, y direction (Fig. (4.3)). Loads were applied at the outer side of the DT geometry, two at the bottom and two at the top.

To simulate the experimental setup of a four-point loading configuration, a force couple was applied at one far end of the specimen. The resulting torsional moment was scaled to obtain a SIF equivalent to the $K_{IC} = 46.8\ \text{MPa}\sqrt{\text{mm}}$ (the fracture toughness of the PMMA).

In order to simulate a more realistic crack tip configuration, an inclined crack front of $c = 4$ was used (Fig. (4.4)). Contact was defined between the crack surfaces as tangential behaviour with 0.5 friction coefficient for rough surfaces.

4.2.4 EVALUATION OF THE CRACK LENGTH INDEPENDENT SIF

The output parameters obtained for each model were the load point displacement y and the applied moment to obtain a SIF equal to that of the aforementioned PMMA fracture toughness. The applied moment could be seen as a concentrated load P with moment arm length w_m in Equation (3.17). Since the SIF, i.e. K_I, was only a function of P in Equation

(3.17), it was possible to evaluate a crack-length-independent SIF using only P, normalised to P_c (the load at $a = 0.5L$).

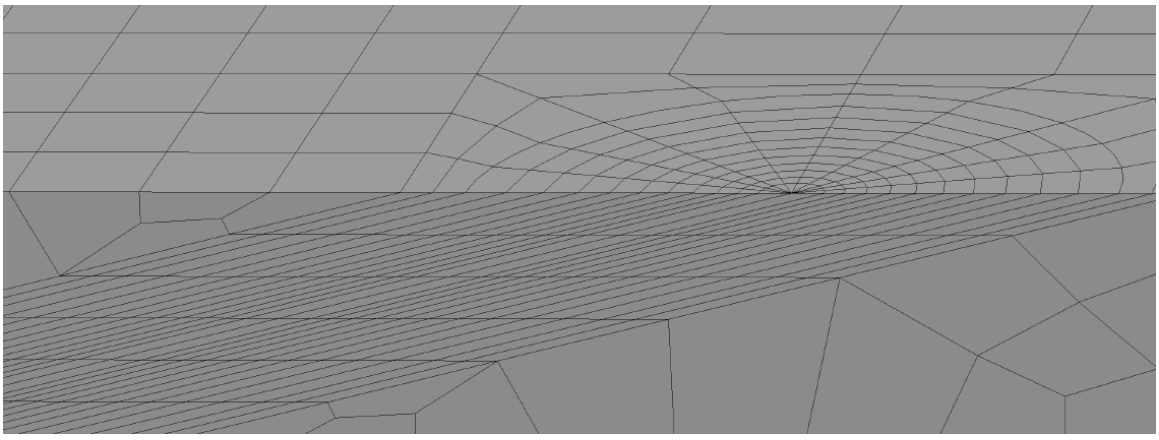

Figure 4.4. Inclined crack tip showing deformation stress, which signifies the crack opening.

4.3 Conclusion

The summary of the CT and DTDCB geometries' modelling process was given in this chapter. Both geometries were modelled using CFEM and XFEM methodology. DT was only modelled using the CFEM, and the Abaqus implementation summary was also given.

Both detailed Abaqus implementations are given in the Appendices sections. The following chapter describes the results that were obtained.

CHAPTER FIVE

RESULTS AND DISCUSSION

This chapter gives the results of the models and the discussion of results is provided. Conventional Finite Element Method (CFEM) and eXtended Finite Element Method (XFEM) results are given for CT and the DTDCB specimen. Further, the DTDCB optimum specimen is studied and the results are also provided.

Finally, the DT results, CFEM, and discussion are also provided.

5.1 Conventional Finite Element Method (CFEM)

5.1.1 COMPACT TENSION SPECIMEN RESULTS (CFEM)

The FEM results were extracted in Abaqus and each value for SIF contour was plotted. This contour is the ring around the crack tip where the J-Integral is evaluated. It is well known that at the crack tip there are singularities. It is for this reason that the contours were chosen further away from the crack tip. The Abaqus results were seen to converge (see fig. (5.2)) after the third contour on the CT specimen, i.e. further away from the crack tip. From Fig (5.2) and Fig (5.5), coloured lines represent contours at each thickness level. Each line represents 15 rings of elements which correspond to contours.

For complete results, the SIF values were taken after the sixth contour, which ensures the accuracy of the results. The high stress concentrations occurring at the crack tip and the loading holes are shown in Fig. (5.1).

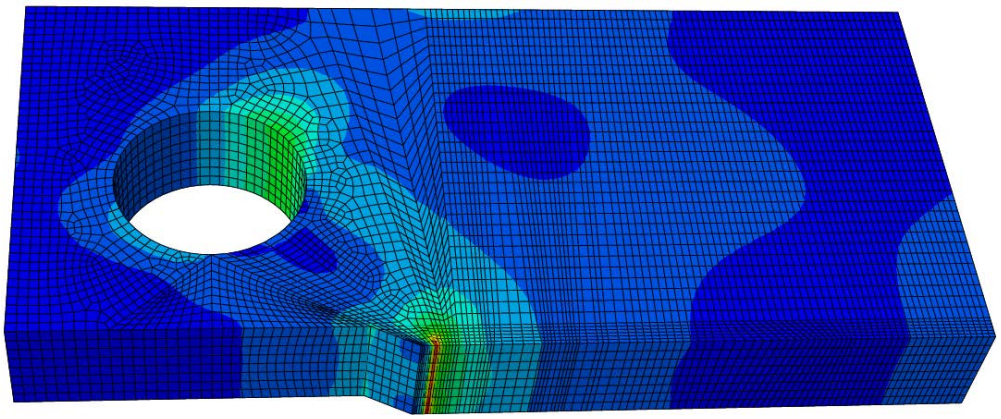

Figure 5.1. CT specimen showing von-Mises stresses.

The analytical results of the SIF were calculated and compared to numerical (Abaqus) results, according to the following equation:

$$K_I = \frac{P}{B\sqrt{W}} f\left(\frac{a}{W}\right) \tag{5.1}$$

where K_I is the SIF, P is applied force, W is specimen width, a is crack length, and B is the breadth of the specimen. SIF, K_I, was found to increase as the crack length increased, as shown in Fig. (5.3). It is worth noting that the analytical results were calculated using Equation (2.40), or Equation (5.1), at each crack length. All equation parameters were measured during the model development in Abaqus.

Both analytical and numerical results were found to correspond, with minor percent error, which is not highly significant. This confirms that the methods can be used further to other different geometries, as the CFEM trend results correspond to the literature.

Since we were evaluating the new geometry, it was necessary to study the geometric factor values. For this reason, the multiple regression was performed using the combination of forward and backward regression after an inversion of Equation (5.1) for: $Y = f\left(\frac{a}{W}\right)$, and

$$Y = \frac{K_I B\sqrt{W}}{P} \tag{5.2}$$

The following variables, based on Equation (2.34) and similar to [7], were used: $\left(\frac{a}{W}\right)$, $\left(\frac{a}{W}\right)^{\frac{1}{2}}$, $\left(\frac{a}{W}\right)^{\frac{3}{2}}$, $\left(\frac{a}{W}\right)^{\frac{5}{2}}$, $\left(\frac{a}{W}\right)^{\frac{7}{2}}$and $\left(\frac{a}{W}\right)^{\frac{9}{2}}$.

The coefficients were calculated with the R-Value which exactly matched 1, as it was expected, since the CT specimen was used as a reference. These showed that the coefficients were explained through a close to 100% degree of accuracy. The final geometrical factor equation was given by:

$$Y = 27.51 - 100.39\left(\frac{a}{W}\right)^{\frac{1}{2}} + 345.29\left(\frac{a}{W}\right)^{\frac{3}{2}} - 710.84\left(\frac{a}{W}\right)^{\frac{5}{2}} + 74.13\left(\frac{a}{W}\right)^{\frac{7}{2}} - 259.26\left(\frac{a}{W}\right)^{\frac{9}{2}} . \tag{5.3}$$

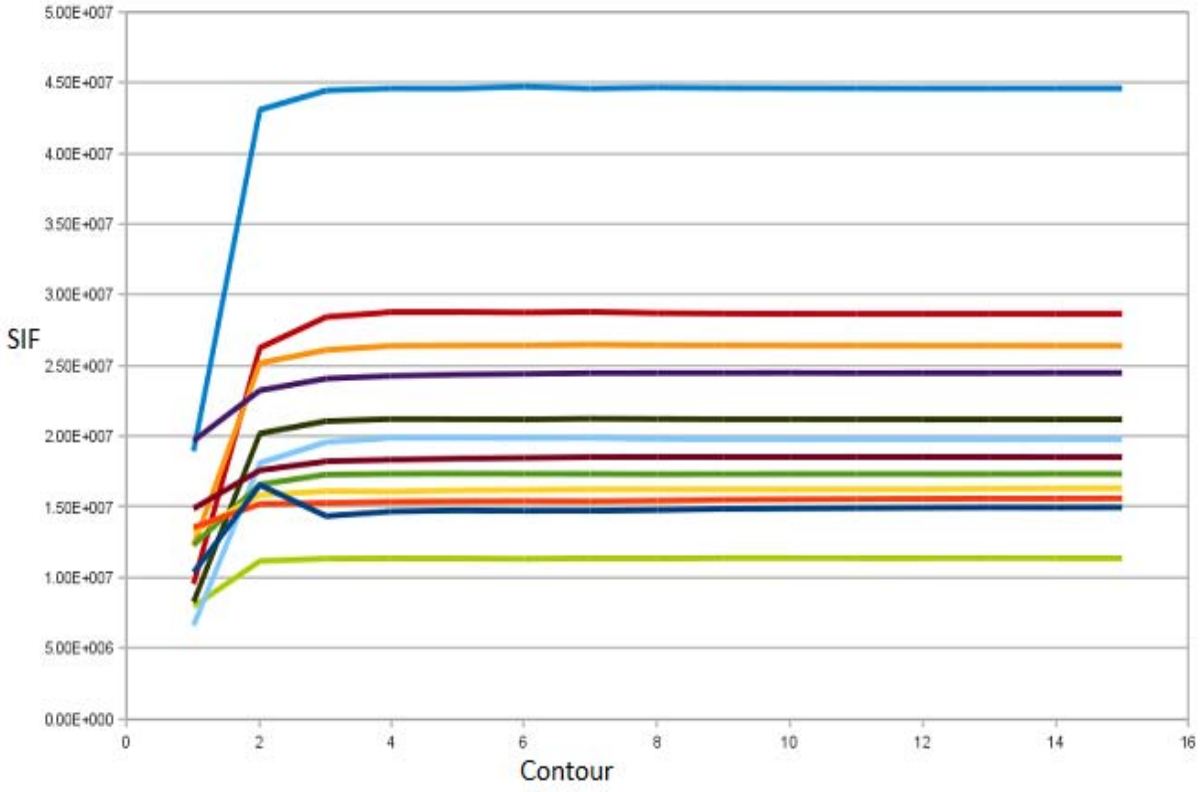

Figure 5.2. The stress contour analysis showing the SIF vs. contour. The SIF converges from the ^{t} third contour.

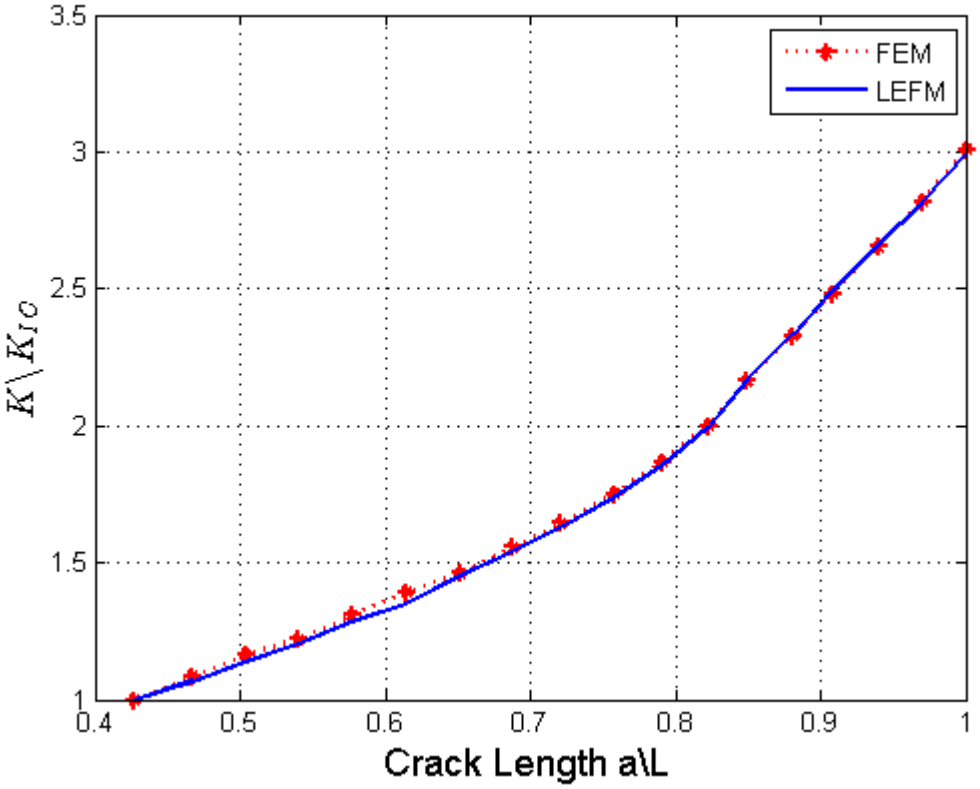

Figure 5.3. Comparison between FEM and LEFM results showing a good correlation. Steel material properties were used to achieve this, see Table (4.2).

5.1.2 DTDCB SIF RESULTS (CFEM)

The results followed the same trend as those that were used and verified to be correct for the CT specimen. In this case, the only difference was in the choice of geometry and the dimensions that were used. The results were compared

with the literature, and they correspond exactly with the literature [46], which showed the SIF decreasing after just above 40mm, point **A**, of the crack length, indicated in Fig. (5.6), until at about 90mm, point **B**, where it started to decrease. The points **A** and **B** can be seen on Fig. (4.2) in Chapter 4. Fig. (5.6) shows a plot of SIF vs. crack length and a comparison to a symmetric part of the DTDCB model.

Fig. (5.4) shows the high stress concentration at the crack tip and the loading points. The high stresses were experienced at the point where the angle started to change, i.e. point 3. This shows that the specimen should be somewhat modified to overcome these high stresses which would cause failure, especially at the loading holes.

The new proposed specimen for laboratory testing is investigated in section (5.3).

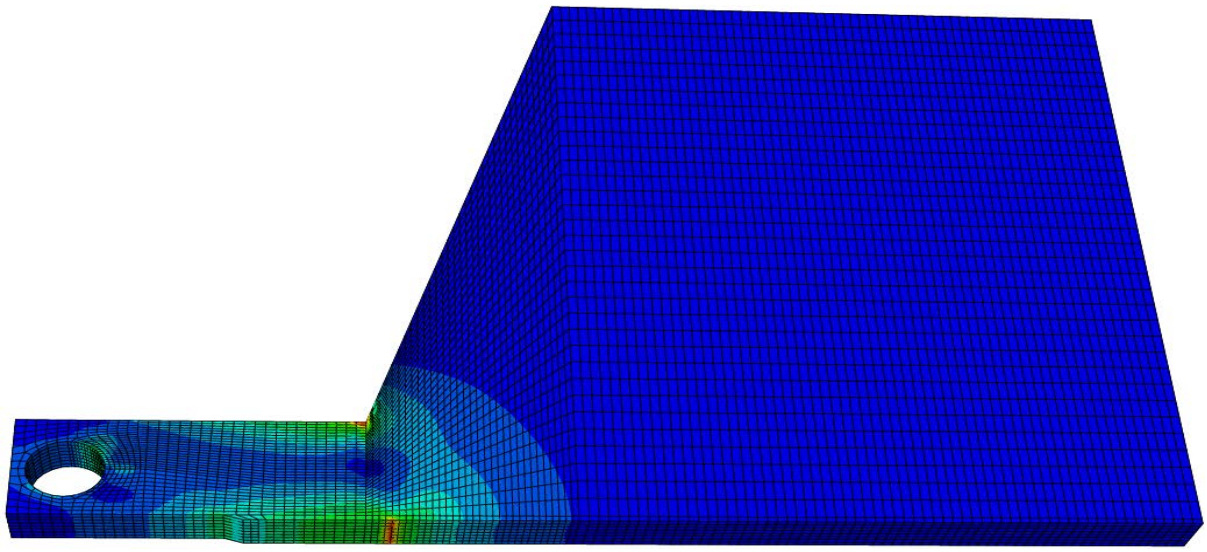

Figure 5.4. DTDCB: Von-Mises Stresses.

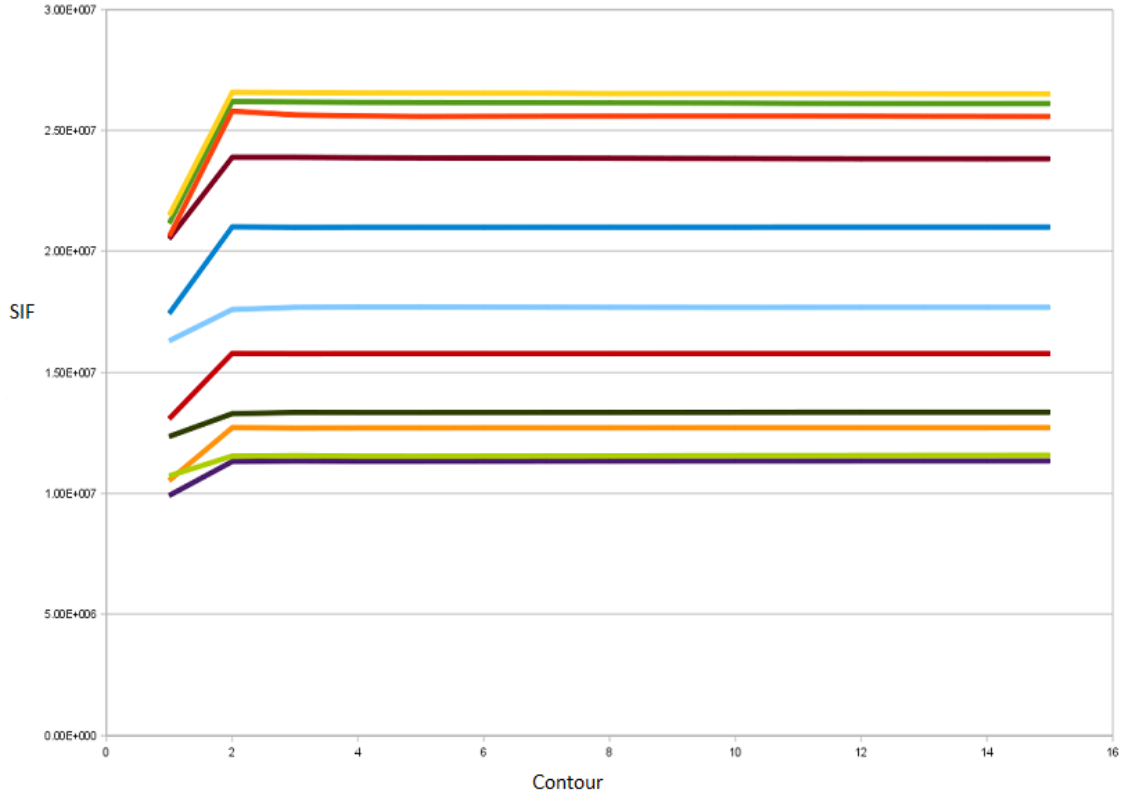

Figure 5.5. DTDCB: Contour plots around the crack tip.

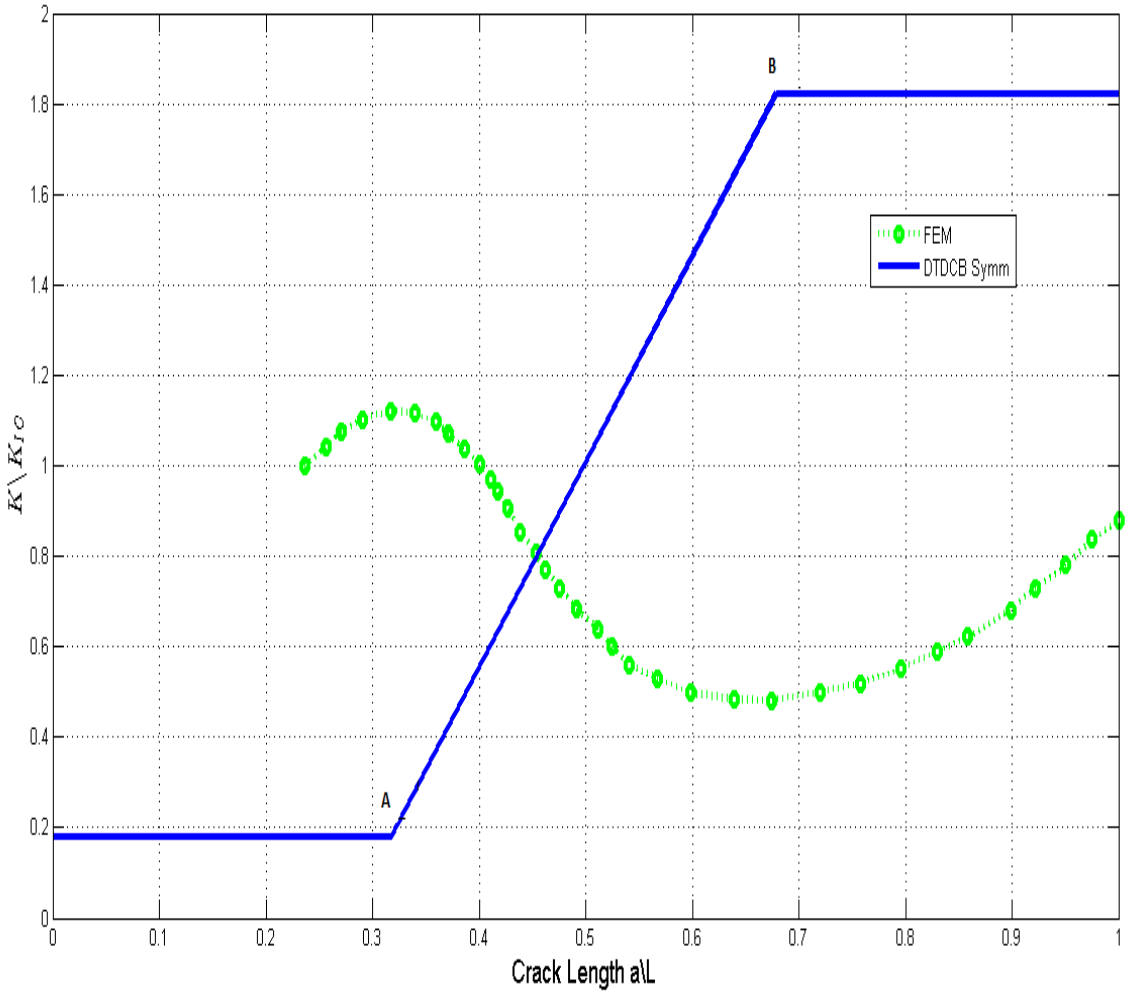

Figure 5.6. DTDCB: Stress intensity factors vs. the crack length. Shows the symmetric part of DT DCB with corresponding ***A*** and ***B*** to the specimen from Fig. (4.2). Similar to CT specimen, steel material properties were used to achieve this, see Table (4.2).

We also performed a regression analysis to find the correction geometric factor which was found to be:

$$Y = -337.9 + 1469.45\left(\frac{a}{W}\right)^{\frac{1}{2}} - 4919.44\left(\frac{a}{W}\right)^{\frac{3}{2}} + 9724.34\left(\frac{a}{W}\right)^{\frac{5}{2}} - 9349.25\left(\frac{a}{W}\right)^{\frac{7}{2}} + 3514.69\left(\frac{a}{W}\right)^{\frac{9}{2}}. \quad (5.4)$$

5.2 Extended Finite Element Method (XFEM)

The XFEM was used to find the point of crack arrest during the crack propagation. This point, based on certain loading conditions, may be regarded as the point where SIF threshold value is determined.

5.2.1 Compact Tension Specimen and the DTDCB (XFEM)

The XFEM SIF was calculated at each crack position in the specimen using the J-integral, similar to the CFEM method. The SIF evaluation in XFEM differed in the sense that the SIF are evaluated in the static or non-moving cracks in order to locate the crack tip, for singularity capturing. The J-integral assumed the nonlinear elasticity, large deformations, which were compatible with the no-load deformation when crack growth occurred [70].

Therefore, the J-integral was applicable only up to the beginning of the crack extension, not to the crack growth [71]. Hence, we expected to experience difficulties in the

converging of a solution, and, hence, SIF evaluation using the XFEM method was found to be impractical to evaluate SIF at this point, and only the point of arrest was of interest. Therefore, the XFEM investigation of SIF was beyond this project's scope.

Fig. (5.7) and Fig. (5.8) show snapshot results during the crack propagation until it arrests at increasing time interval of the CT specimen - Fig. (5.7) and DTDCB specimen Fig. (5.8) respectively, as shown below. The blue colour shows less stresses, whereas the red shows high stress concentrations. The crack in both specimens propagates until it reaches the point of arrest.

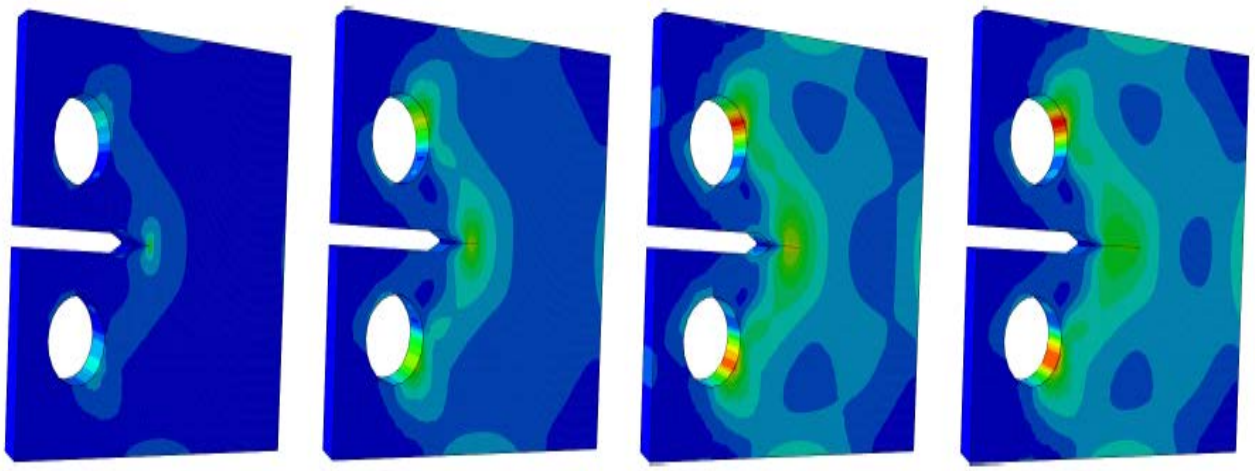

Figure 5.7. Snapshot of CT crack propagation and von-Mises stress. The attention is drawn to the advancing crack tip (crack displacement) across the specimen until it arrests.

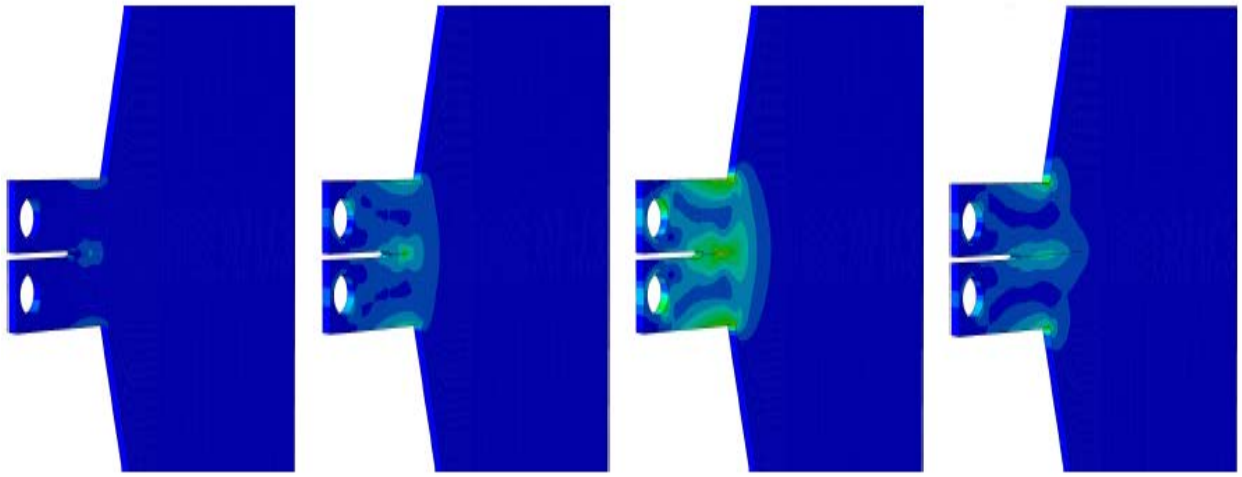

Figure 5.8. Snapshot of DTDCB crack propagation and von-Mises stress. The crack propagates (crack displacement) across until it reaches the point of arrest at the region of increasing height.

The point of arrest in the DTDCB specimen was found to be at the region of increasing height, and this was verified using the XFEM method, Fig. (5.8). As the crack grows, high stresses are experienced at the loading holes and the region of increasing height. Therefore, it was necessary to obtain an optimised geometry that might be suitable for use in the laboratory, see the next section.

5.3 Optimised DTDCB Geometry Model Investigation

Note that the rest of this section will refer to a DTDCB (points 1 to 6 and points **A** and **B**) as shown in Fig. (4.2) in Chapter 4.

The final specimens proposed are shown in Fig. (5.9) and Fig. (5.10). To obtain these geometries, the region that was modified was the region of high stress concentration shown in Fig. (5.4) in the previous section. From Fig. (4.2), point 3 was reduced to correspond to point 2 in both figures. Fig (5.9) was reduced further from 41.2 to 37mm in order to investigate the influence of larger area between loading points and the initial crack location. Both the reduction in height and specimen length reduction were investigated.

Fig. (5.9) shows a reduced specimen between loading holes and point 2, points 2 and 3, and a further deduction in points 4 and 5, from Fig. (4.2). The results of this kind caused the specimen SIF to follow a similar trend to the CT specimen, Fig (5.11), i.e., increasing SIF.

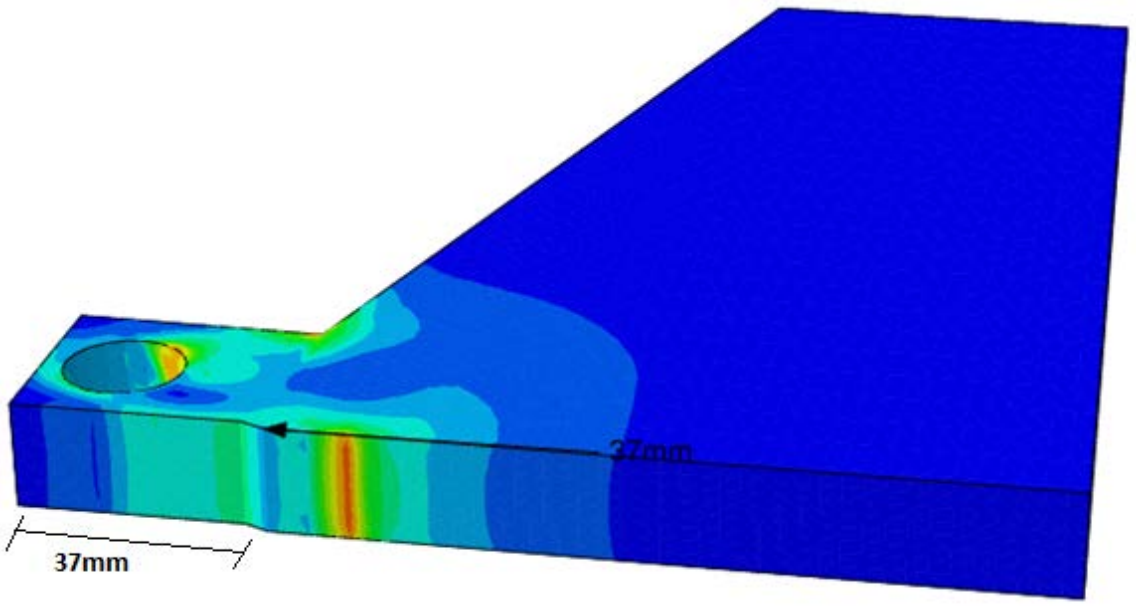

Figure 5.9. DTDCB: Reduced proposed specimen configuration.

Further investigations were required to find an optimum decreasing SIF specimen. For this reason, the specimen was not reduced between the loading holes and point 2. But it was reduced between points 2 and 3, as was the height between points 3 and 4. It was not reduced between loading points and point 2.

The resulting specimen geometry produced decreasing SIF from point A but started to increase eventually in the middle of the increasing height, between points 3 and 4.

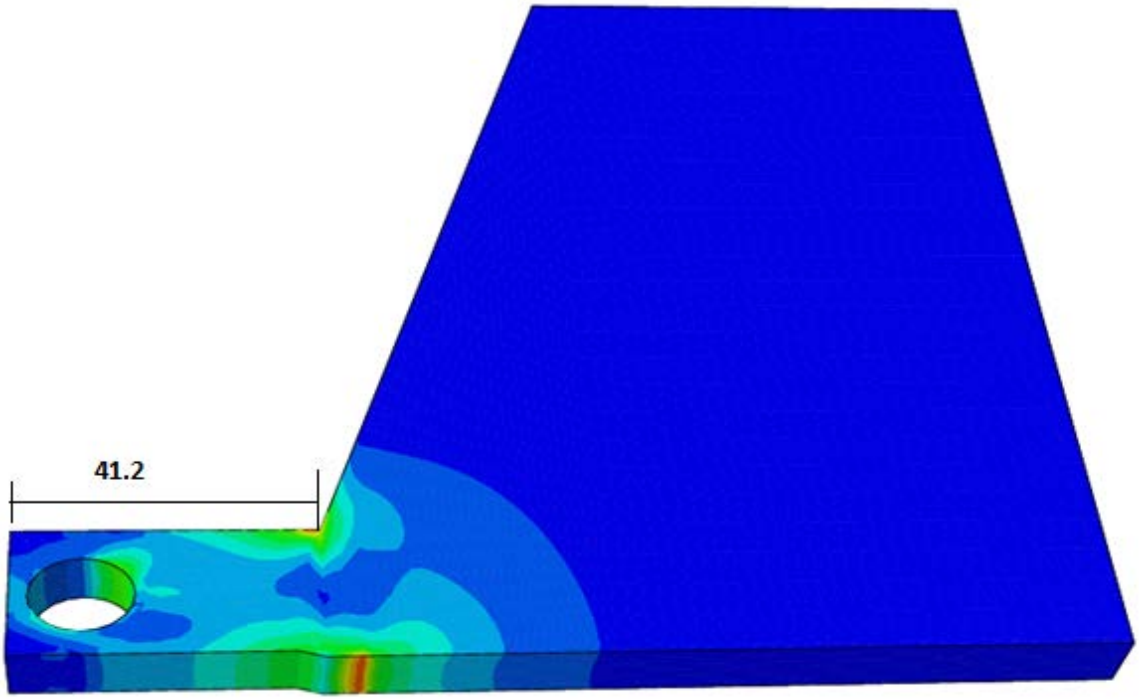

Figure 5.10. DTDCB: Shifted proposed specimen configuration.

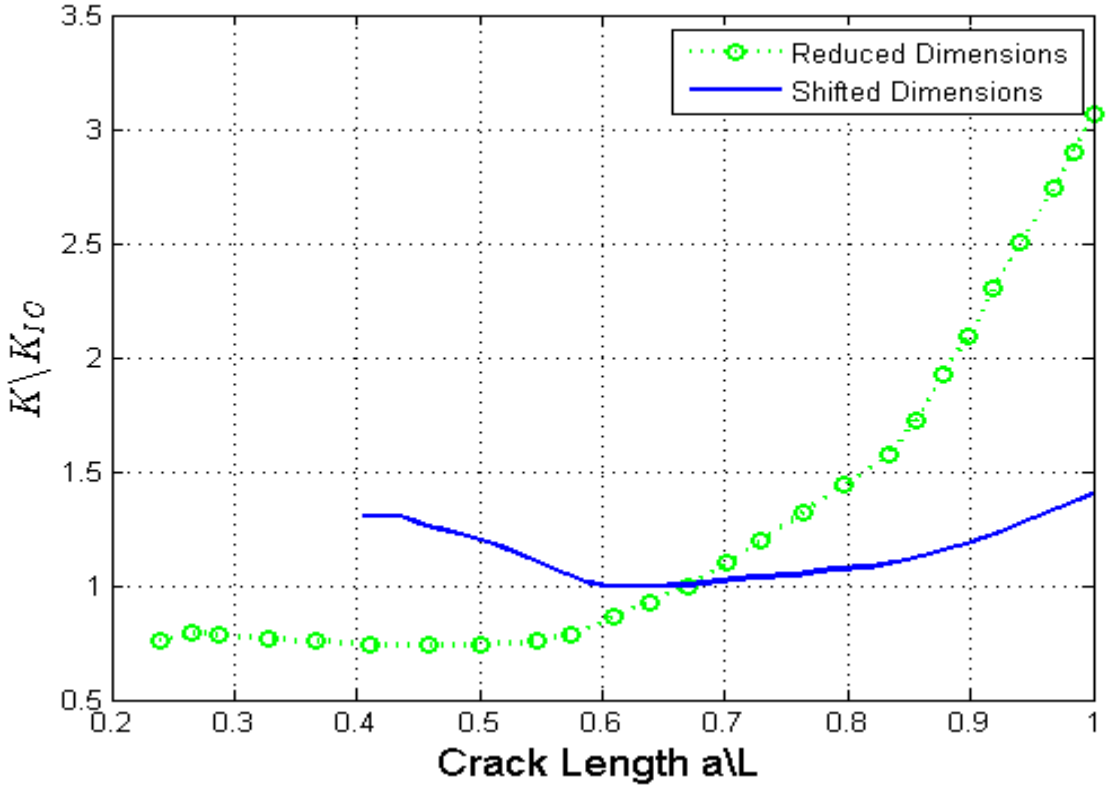

Figure 5.11. DTDCB: Shifted and reduced SIF comparison.

In conclusion, the optimum geometry may only be found if the DTDCB specimen geomerty is only shifted and not reduced, see explanation above. This geometry needs more detailed future investigations in order to obtain a suitable reduced DTDCB geometry.

5.4 Double Torsion Results

Figures 5.12, 5.13 and 5.14 show the normalised force vs. crack length results for three different specimens of length ratios *2W*, *3W* and *4W* respectively.

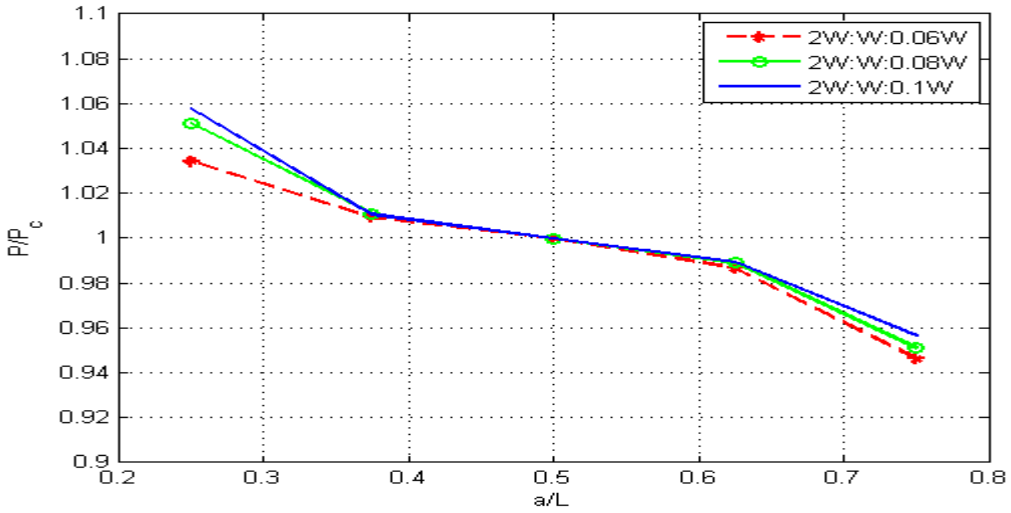

Figure 5.12. Normalised force vs. crack length comparison of thickness of Length L = 2W.

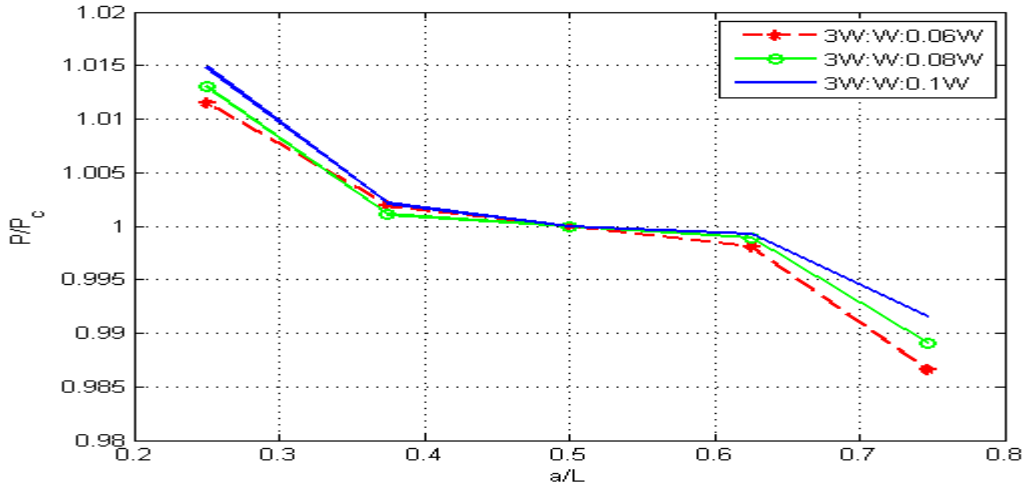

Figure 5.13. Normalised force vs. crack length comparison of thickness of Length L = 3W.

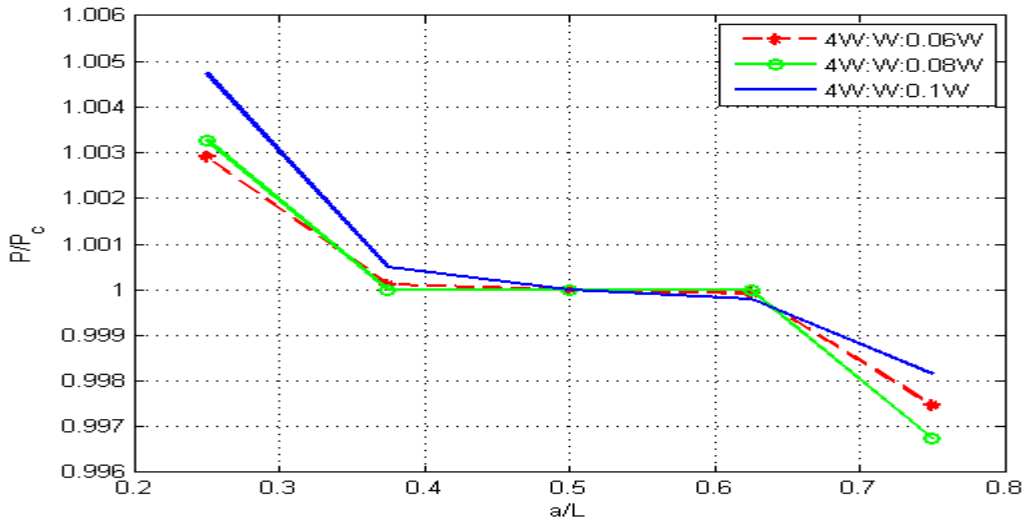

Figure 5.14. Normalised force vs. crack length comparison of thickness of Length L = 4W.

Similarly, Figures 5.15, 5.16 and 5.17 show the normalised force vs. crack length results for three different specimen thickness ratios of *0.06W, 0.08W* and *0.01W* respectively. From Figures 5.12, 5.13 and 5.14 it can be seen that a thinner specimen configuration yields a more crack-length-independent geometry. Figure 5.13, for example, $L = 3W$, shows a relatively constant SIF in the range *0.37W* to *0.75W*. That is, the SIF are closer to 1 than compared to the other figures. Comparing Figures 5.15, 5.16 and 5.17, the thinner specimen configuration $d = 0.06W$ shows the constant SIF over the middle of the specimen. That is, the P/P_c value is closer to 1 as compare to the other figures.

From Figures 5.15, 5.16 and 5.17, it can be seen that the specimen that is closest to producing constant SIF lies between $L = 3W$ and $L = 4W$ thickness.

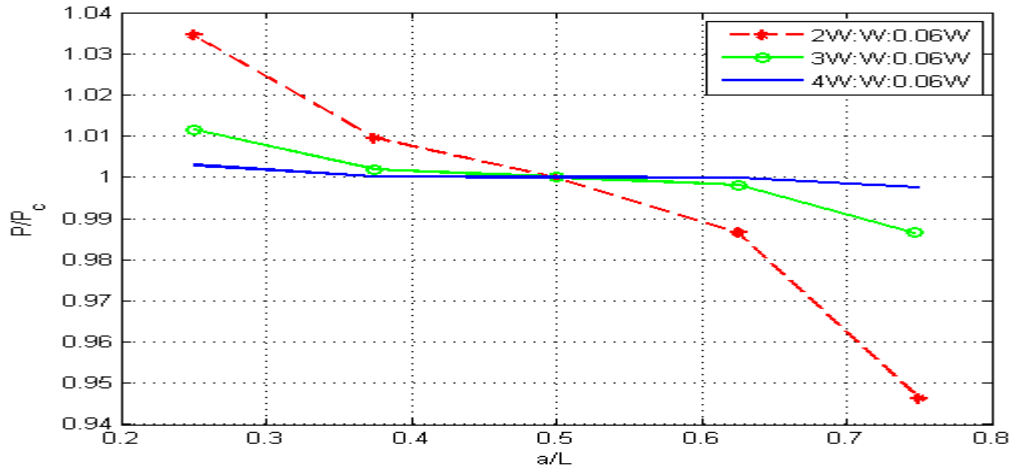

Figure 5.15. Normalised force vs. crack length comparison of thickness of Length L = 2W.

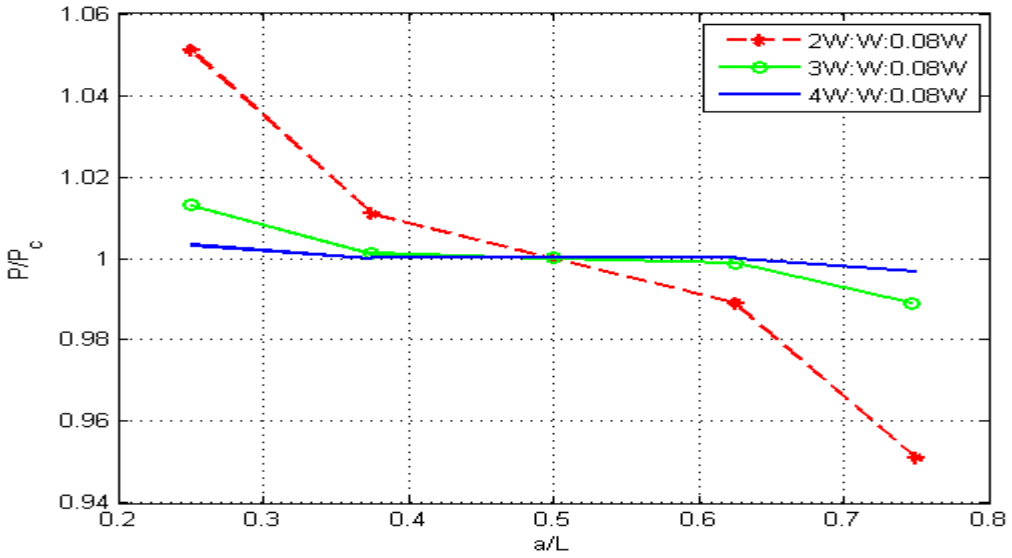

Figure 5.16. Normalised force vs. crack length comparison of thickness of Length L = 2W.

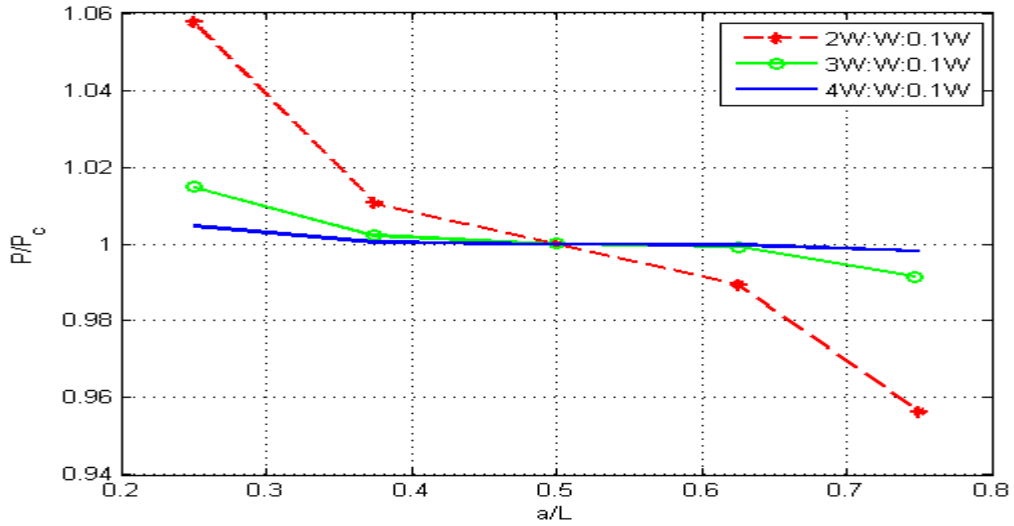

Figure 5.17. Normalised force vs. crack length comparison of thickness of Length L = 2W.

Based on these two comparisons, involving length and thickness of the specimen geometries, respectively, we propose that the optimum specimen geometry should be of the order $3.5W:W:0.06W$.

5.5 Summary

In this chapter, both CFEM and XFEM results were provided. These FEM methods were applied to both CT and the DTDCB specimen geometries. The CFEM was applied in order to study SIF, and the XFEM was applied in order to find the point of arrest during the decreasing SIF, which forms the point of importance to this project. CT specimen was used as a reference to validate the results.

DT specimen results were also provided, where CFEM was applied. Comparison between the thickness and the specimen lengths was provided in order to find optimum specimen geometry.

The next chapter provides an overall discussion of the results.

CHAPTER SIX

DISCUSSION

This project was motivated by the two aims, a crack length decreasing SIF and a constant SIF specimen, which were proposed before [7] and [6] in order to answer the questions that were raised. It also sought to contribute to the fracture mechanics literature. The questions were answered by investigating a decreasing SIF specimen using FEM and XFEM methods and investigating a DT geometry using the CFEM method. Therefore, this chapter is split into two sections; firstly, a discussion of the crack length decreasing SIF, where the CT and DTDCB specimen were both discussed in detail. The second section was aimed at a discussion of a constant SIF specimen, DT, where the modelling results were discussed. Before we begin, a summary of the project will be given.

6.1 Summary of the project

The finite element method was chosen as a method of modelling in order to investigate the geometries in question. Two FEM methods were applied to the geometries depending on the aim that was expected for each model. Therefore, CFEM was applied to all specimens in order to investigate the SIF. Since the aim of investigating the decreasing SIF geometry was to obtain a point of arrest, referred to as stress intensity fatigue threshold, it was necessary to apply the XFEM method, since it is used on dynamic propagating cracks. XFEM was applied to the CT (for verification purposes) and DTDCB specimen to obtain the point of arrest where the crack will not grow. This point may be referred to as a SIF threshold value, which is important in fatigue studies and is known for its fatigue life prediction discussed in Chapter 2. Despite the XFEM SIF not converging, owing to limitations in Abaqus [10], the method does have a bearing on the

suitability of finding the point of arrest for given loading conditions. These can be summarised in the table below:

CT	DTDCB	DT
CFEM	CFEM	CFEM
XFEM	XFEM	-

Table 6.1. Three specimens showing the FEM methods which were applied to the specimen.

6.2 CT Specimen and DTDCB Specimen

Since the CT specimen is a standard well-known ASTM specimen, it was necessary to use it to verify the FEM models. For this reason, CFEM and XFEM were first applied to the CT specimen, and the results were compared to the analytical solution. Further, the regression analysis was applied to find the geometric factor of the model.

Contour integral results were found to converge at the third contour, and the average was used to find the resulting SIF. This SIF was plotted against the crack length, and the results were compared to the analytical solutions. Furthermore, the XFEM was applied to the geometry to find the point of arrest. This was found to be useful on the geometry of interest, the DTDCB, in order to find the point of no crack growth when the stresses decrease.

DTDCB geometry was found and the FEM methods were applied in order to investigate the geometry. This geometry brings an important contribution to the literature on the subject. Previously, CT-specimen-breadth increase was investigated [7], and it did not have much success because of the failure, especially at the loading holes. This project

rather considered a different approach, based on the recommendation from Rosie et al. [7] where the change in height was investigated. A promising decreasing SIF geometry was obtained and investigated using FEM, and XFEM analysis was applied to this geometry. These have been demonstrated in Chapter 5, where both methods were applied. The decreasing range of SIF was found to be in the region of $0.8W < a < 1.8W$. It was in this region where the point of arrest was found using XFEM, and this point can be utilized in fatigue investigation to predict the fatigue life, using the Paris equation discussed in Chapter 2.

These decreasing SIF results can be explained as follows. The fatigue crack was expected to grow in a direction perpendicular to the direction of the maximum principal stress. This has been demonstrated in section (5.2.1), where XFEM was used and the snapshot of crack propagation was taken. As the crack propagates, before it reaches $0.8W$ length, the SIF was increasing owing to both constant width and breadth in that region. After this region, the height is increased at an inclined angle $\theta = 73.3^{\circ}$. This region opposes the applied force, and hence decreases SIF as the height was increased. The observation continues until stress intensity was lowered and the crack could no longer propagate. Therefore, the crack was expected to arrest at this region, and hence the threshold SIF value could be determined.

Owing to high stresses that were experienced at the loading holes, it was necessary to optimize this geometry in order to obtain a specimen that would avoid fretting fatigue and hence failure at the loading holes. Therefore, further analysis was done, and the optimum specimen geometry was investigated. This opens doors to further future investigations to find a further small geometry, since the DTDCB had larger dimensions. The larger dimensions may prove to be impractical for different materials, especially brittle

materials, since the crack will be observed in long range for this type of geometry. Therefore, future investigations should rather focus on optimizing this geometry further.

CFEM, applied to a similar CT specimen, was used to investigate this proposed geometry. Two important points in the geometry, points ***A*** and ***B,*** were found, where the specimen produced decreasing SIF. Contour analysis was investigated at the region surrounding the crack tip, and the contours were found to converge from the third contour. The average was taken from the sixth contour in order to find the resulting SIF. This helped to investigate the convergence of the FEM solution.

It was interesting to find that, in the regions where the specimen height was constant, increasing SIF were produced, and these were the regions which were similar to CT, which has a constant height and breadth and produces increasing SIF.

When the specimen is loaded, high stresses occur at the loading points of the specimen and at point 3, where the height started to increase. This is owing to the regions where the specimen behaves similar to CT, when SIF are increasing. Therefore, for future investigations, it may be necessary to include a pre-crack up to point ***A*** and begin with the investigations. Owing to a long distance to reach point ***A***, 40mm, it is also possible to find an optimum specimen geometry that will prevent high occurring stresses. These observations can then be utilized in fatigue tests which use the continuous load-shedding steps. The advantage of this would be that the DTDCB specimen can be left to run to arrest without continually lowering the applied stress, since this specimen lowers the stress intensity at the crack tip.

In this project, we investigated two optimum geometries using the DTDCB specimens, see section 5.3. From these investigations, it was found that the optimum specimen

geometry could be found only when the specimen was reduced in points 2 and 3; and the height, between points 3 and 4. The specimen should not be reduced between the loading points and point 2, since it was found to be have similar to the CT specimen, where increasing SIF were produced.

6.3 DT Specimen

The DT geometry was modelled using only the CFEM methodology. The aim of investigating this geometry was to answer the second question of this project, which was to contribute to understanding the influence of geometry on a constant SIF of the DT geometry, which is mostly used in brittle material investigations. The compliance is linear, and hence the SIF over the middle of the DT specimen is independent of crack length. This geometric investigation was done by applying FEM to study the influence of length and thickness on SIF and obtain optimum dimensions which may be used in DT investigations.

Theoretical background on SIF derivation was given in Chapter 3, which was followed by the modelling process in Chapter 4. The results were given in Chapter 5.

6.3.1 RESULTS OBSERVATIONS

As aforementioned, SIF is constant in the middle region of the specimen, and this was also observed in this project. Firstly, comparisons of length ratios, for different thicknesses, were given in Figures 5.12, 5.13 and 5.14. From the length ratio 2W, not much difference was observed - only the specimen of 0.06W, which was close to the range of constant SIF. It was mentioned in Chapter 4 that there is an equivalence relation between SIF and the normalized force ratio P/P_c.

For the specimens of length 3W, the SIF were observed to be in a region close to $\frac{P}{P_c} = 1$, which was the region of constant SIF. This was observed in a specimen of thickness 0.08W.

The last specimens that were compared here were the specimens of length ratio 4W. The thicknesses of 0.06 W and 0.08 W were both observed to produce quite a constant SIF range in the middle region, and the thickness of 0.08W was even more constant as compared to 0.06W.

In overall length ratio comparison, the thickness ratio of 0.1 W did not seem to give a constant SIF regime. Furthermore, it was observed that the longer the specimen length, the closer the specimen was to achieving constant SIF. Hence, there was an eed to compare specimens of different thicknesses.

Secondly, comparisons of thickness ratio, for different lengths, were given in Figures 5.15, 5.16 and 5.17, where the normalized force vs. crack length results were given. Starting with the thickness of 0.06W, it was found that the longer specimen of 4W was the closest to the constant SIF region, and, hence, this supports our previous observations where length ratios were compared.

Similar observations were made when comparing thicknesses of 0.08 W and 0.1 W. The length ratios of 3W and 4W were observed to be close to producing constant SIF.

Therefore, based on these observations, a detailed discussion is given in the next section.

6.3.2 DT SUMMARY

Comparison between the DT specimen lengths and thicknesses was useful in predicting a suitable constant SIF vs. crack length geometry. Comparison between the ratios of lengths of *2W*, *3W* and *4W* shows that the specimen geometry should lie between thicknesses 0.06 W and 0.08 W. Comparing thickness ratios *0.06W, 0.08W* and *0.01W* suggested that the geometry should be in the range 3W and 4W.

Thin specimen will require less applied force to propagate a crack. This means that, for brittle material, we can be able to propagate the crack at lower stress levels, and, hence, the crack propagation will be stable. The longer-range specimens of 3W and 4W suggest that the specimen crack growth can be monitored over the long range when stresses are relaxed, since they are far from the loading points. Therefore, the combination of the two, i.e. thin and long specimen geometry, suggests that it is possible to obtain stable and constant specimen geometry. Hence, the specimen of *3.5W: W :0.06W* will be a good choice.

The shorter specimens give a shorter constant SIF range, and this has been found to be owing to edge effects [6]. With longer specimens, for example L = 4W, the edge effect is reduced; however, it is difficult to propagate a crack in a longer specimen. Hence, the use of L = 5 W, or more, was omitted in this project. If, on the other hand, the longer specimen is used, normally, the side grooves are applied. However, side grooves also provide stress concentrations [69].

CHAPTER SEVEN

CONCLUSION AND FUTURE RECOMMENDATIONS

Based on the results obtained in this project and the discussion that followed, the following conclusions and recommendations can be drawn from each specimen.

This work was split into two sections to fulfil the project's objectives. The first section dealt with the investigation of the SIF threshold value using the CT as the reference, and DTDCB specimen was developed. The second section dealt with the standardization of the DT methodology studying the thickness and the length effect to constant SIFs of the specimen.

7.1 CT SPECIMEN AND DTDCB SPECIMEN

7.1.1 Conclusion

The combination of CFEM and XFEM is successfully employed to develop a crack growth specimen capable of producing the decreasing stress intensity factors to facilitate easy determination of fatigue threshold values, ΔK_{th}. The CT specimen acted as a good reference to verify the methods. A good correlation between SIF corresponds well with the literature.

The DTDCB specimen geometry facilitates the decrease of SIF from the point of increasing height up to the end of the height, where SIFs eventually increase. This means

that the part from where the specimen is loaded and the small section at the end of the specimen behave like the CT specimen, i.e., SIF increases owing to the constant height similar to the CT specimen. Only in the middle part was there a decrease in SIF as expected.

The point of arrest, which may be referred to as the threshold value, was obtained using the XFEM method. The crack was observed to grow up until the middle of the portion where the height was increased.

7.1.2 Future Recommendations

Based on the observations above, we were able to determine an optimum geometry from the DTDCB model. The optimum geometry will need to be tested in the laboratory, using different types of materials.

Further, more geometric investigations need to be undertaken. For example, the microscopic investigation as well as different boundary conditions need to be investigated.

7.2 DT SPECIMEN

7.2.1 Conclusion

This project investigated an optimum specimen geometry using nine different specimen geometry configurations. The analysis was undertaken in the FE environment to obtain a relationship between the SIF and crack length. An ideal specimen would yield a crack length independent of SIF.

It was found that a thinner specimen resulted in producing constant SIF. It was also found that a thinner specimen produced a more constant SIF regime. Similarly, it was also observed that the longer specimen resulted in a more constant SIF regime. This is in agreement with Trantina (2006) [61] and Tait (1987) [69], who suggested that the SIF remains constant over $0.18 < a/L < 0.78$ range.

A comparison of the results suggests that an optimum specimen geometry exists around 3.5W:W: 0.06W.

7.2.1 Future Recommendations

There are still many aspects to be investigated for the CT geometry to be a standard model. For example, the standard dimensions for different materials, load point deflections, and out-of-plane deformations still need to be investigated.

Laboratory testing needs to be investigated. For example, with the long test specimen the deflection at the middle of the specimen will occur. It is crucial to find out how this deflection will affect the constant SIF.

REFERENCES

[1] H.L. EWALDS and R.J.H. WANHILL. Fracture Mechanics. *London*: Edward Arnold 1989.

[2] J.D.G. SUMPTER and J.S. KENT. Prediction of ship brittle fracture casualty rate by a probabilistic method. *Marine Structures*, 8(17):575-585, 2004.

[3] H.S. REEMSYNDER. Ships that have broken in two pieces – World War II US maritime commission construction. *Bethlehem Steel internal memo*, 1402-1b, 1990.

[4] A.A. GRIFFITH. Philosophical transactions of the royal society of London. *Series A, Containing Papers of a Mathematical or Physical Character* 221:163-198, 1921.

[5] A.D. KARSTENSEN, A. HORN and M. GOLDTHORPE. Local approach predictions of fracture toughness behavior in real multi pass welds using thermal simulation specimens. 2nd International Symposium on High Strength Steel (press), Stiklestad, Verdal, Norway, 23-24 April (2002).

[6] T.H. BECKER. Understanding and modelling damage and fracture in nuclear grade graphite. *PhD Thesis*. University of Cape Town 2011.

[7] K.A. ROSIE. Fatigue Threshold. Masters thesis, University of Cape Town, 2009.

[8] S.T. ROLFE and J.M BARSOM. Fracture and fatigue control in structures. *Applications of Fracture Mechanics* 1977.

[9] W.F. BROWN, Jr., Editor. Review of developments in plane strain fracture toughness testing. *ASTM STP* 463, 1970.

[10] ABAQUS, User's Manual, Version 6.10. *ABAQUS Inc., Providence, Rhode Island*, 2011.

[11] ASTM. 2007. ASTM standard test method for measurement of fatigue crack growth rates (E647-05). *Annual Book of ASTM Standards*, 03-01: 692-735.

[12] W. SCHÜTZ. A History of Fatigue. *Engineering Fracture Mechanics*, 54(2): 263 – 300, 1996.

[13] Y. IINO. Local fatigue damage accumulation around notch attending crack initiation. *Metallurgical and Materials Transactions*, 26(6):1419-1430, 1995.

[14] P.C. PARIS, M.P. GOMEZ, and W.E. ANDERSON, A Rational Analytic Theory of Fatigue. *The Trend in Engineering*, 13:9–14, 1961.

[15] A.A. GRIFFITH. the phenomena of rupture and flow in solids, Philosophical Transactions of the Royal Society of London Series A, *Containing Papers of a Mathematical or Physical Character* 221:163–198, 1921.

[16] D. BROEK. The Practical Use of Fracture Mechanics. *Fracture research Inc*., Galena, OH, USA, 1988.

[17] J.R. RICE. A Path Independent Integral and the Approximate Analysis of Strain Concentration by Notches and Cracks. *Journal of Applied Mechanics*, 35:379-386, (1968).

[18] S. COURTIN, C. GARDIN, G. BEZINE and H.BEN HADJ HAMOUDA. Advantages of the J-integral approach for calculating stress intensity factors when using the commercial finite element software ABAQUS. *Engineering Fracture Mechanics.* 72:2174-2185, 2005.

[19] J.M. SVVOBODA. Fatigue and Fracture Toughness of Five Carbon or Low Alloy Cast Steels at Room or Low Climate Temperature (Part II). *Carbon and Low Alloy Steel Technical Research Committee Steel Founders' Society of America*. May 1983.

[20] K.K. RAY, N. NARASAIAH and S. TARAFDER. Comparative assessment of fatigue-thresholds estimated by short and long cracks. *Fracture of Nano and Engineering Materials and Structures*. Pp 221-222, 2006.

[21] N.E. FROST and D.S. DUGDALE. The propagation of fatigue cracks in test specimens. *Journal Mechanics and Physics of Solids*, 6:92-110, 1958.

[22] S. PEARSON. Initiation of fatigue cracks in commercial aluminium alloys and the subsequent propagation of very short cracks. *Eng Fract Mech* 7:235–47, 1975.

[23] A.M. RONALD. The use of notched beams to establish fracture criteria for beryllium. UCRL-52866. *Lawrence Livermore Laboratory,* 1980.

[24] M. PERRA and I. FINNIE. Fracture-toughness tests on a high-strength beryllium from room temperature to 3000 °C. *UCRL-51774 Lawrence Livermore Laboratory*. 1975.

[25] T.H. HYDE, M. SABER and W. SUN. Testing and modelling of creep crack growth in compact tension specimens from a P91 weld at 650 ^{0}C. *Engineering Fracture Mechanics*. 77(15):2946-2957, 2010.

[26] S.L. LAHAM. Stress Intensiy Factor and Limit Load Handbook. *British Energy Generation Ltd*. Issue 2, 1998.

[27] T.H. BECKER. An Evaluation of a Double Torsion Technique. *Experimental Mechanics*. 2011.

[28] T.H. BECKER, T.J. MARROW and R.B. TAIT. An Evaluation of the Double Torsion Technique. *Experimental Mechanics*. 51:1511–1526, 2011.

[29] J. FISH and T. BELYTSCHKO. A first course in Finite Elements. *John Wiley and Sons, Ltd*, 2007.

[30] D.M. TRACEY. Finite elements for determination of crack tip elastic stress intensity factors. *Eng. Fracture Mech*, 3:255-266, 1971.

[31] I. NISTOR, O. PANTELE and S. CAPERAA. Numerical implementation of the extended finite element method for dynamic crack analysis. *Advanced in Engineering Software*, 39:573-587, 2008.

[32] N. SUKUMAR. Meshless Methods and Partition of Unity Finite Elements. PhD thesis, Department of Civil and Environmental Engineering, University of California, One Shields Avenue, Davis, CA 95616. U.S.A, 2003.

[33] I. BABUSKA and Z. ZHANG. The partition of unity method for the elastically supported beam. *Computer Methods in Applied Mechanics and Engineering*. 152(12):1-18, 1998.

[34] B. MORAN, N. SUKUMAR, N. MOES and T. BELYTSCHKO. Extended finite element method for three-dimensional crack modelling. *International Journal For Numerical Methods In Engineering*, 48:1549 1570, 2000.

[35] T. BELYTSCHKO and T. BLACK. Elastic crack growth in finite elements with minimal remeshing. *International Journal for Numerical Methods in Engineering*. 45(5): 601-620, 1999.

[36] M.J. MCNARY. Implementation of the extended finite element method (xfem) in the abaqus software package. *Master of science in mechanical engineering*, Georgia Institute of Technology, 2009.

[37] E. GINER, N. SUKUMAR, J.E. TARANCON and F.J. FUENMAYOR. An abaqus implementation of the extended finite element method. *Engineering Fracture Mechanics*, 76:347-368, 2009.

[38] J. DOLBOW, N. MOES and T. BELYTSHKO. A finite element method for crack growth without remeshing. *INTERNATIONAL JOURNAL FOR NUMERICAL METHODS IN ENGINEERING*, 46:131-150, 1999.

[39] Y. PRAWOTO. Application of Linear Elastic Fracture Mechanics in Materials Science and Engineering. *Lulu Enterprise*, Raleigh 2011.

[40] p. Areias, n. Van goethem and E.B. PIRES. A damage model for ductile crack initiation and propagation. 2010.

[41] J. SHI, D. CHOPP, J. LUA, N. SUKUMAR and T. BELYTSCHKO. Abaqus implementation of extended finite element method using a level set representation for three dimensional fatigue crack growth and predictions. *Eng. Fracture Mechanics*. 77:2840-2863, 2010.

[42] L. XUE and T. WIERZBICKI. Ductile fracture initiation and propagation modelling using damage plasticity theory. *Engineering Fracture Mechanics*, 75:3276-3293 2008.

[43] R.L. TOBLER. A numerical and experimental verification of compliance functions for compact specimen. *Engineering Fracture Mechanics*. 21(3):547-556, 1985.

[44] Y. PRAWOTO. Designing steel microstructure based on fracture mechanics approach. *Materials Science and Engineering*. 507:74-86, 2009.

[45] G. IRWIN. Analysis of stresses and strains near the end of a crack transversing a plate. *Journal of Applied Mechanics*. 24:171-183, 1957.

[46] F. R. DESHAYES and W. H. HARTT. Development of a fatigue Crack Growth Rate Specimen Suitable for a Multiple Specimen Test Configuration. Fracture Mechanics: Twenty-Third Symposium, ASTM STP 1189, Ravinder Chona, Ed. *American Society for Testing and Materials*, Philadelphia. 598-618, 1993.

[47] S. MOSTOVOY, P. B. CROSLEY and E. J. RIPLING. Use of Crack-Line-Loaded Specimen for Measuring Plane-Strain Fracture Toughness. *Journal of Materials.* 2(3):661-681, 1967.

[48] M.S. ATTIA, A. S. MAHMOUD, M.M. MEGAHED and A.A. RADWAN. Numerical investigations of the stepped double torsion fracture toughness specimen. *Engineering Fracture Mechanics*. 77:3359-3367 2010.

[49] N. YOSHITAKA, M. KAZUYA, H.C. NAOKI, Y. TETSURO, K. KATSUHIKO and M.B. PHILIP. Influence of relative humidity on fracture toughness of rock: Implications for subcritical crack growth. Solids and Structures. 49:2471–248 2012.

[50] M.H. LEWIS and B.S.B. KARUNARATNE. Determination of High-Temperature KI-V Data for Si-Al-O-N Ceramics. *American Society for Testing and Materials*, 13 – 32, 1981.

[51] T.H. BECKER, R.B. TAIT and T.J. MARROW. Damage, crack growth and fracture characteristics of nuclear grade graphite using the double torsion technique. *Journal of Nuclear Material*. 32 – 43 2011.

[52] J.R. FULLER. An evaluation of the double-torsion testing analysis. Fracture mechanics applied to brittle materials, ASTM STP 678. *American Society for Testing and Materials.* 1979.

[53] S. BASKARAN, S.B. BHADURI and D.P.H. HASSELMAN. Effect of crystallites on subcritical crack growth and strain-rate sensitivity of strength of cordierite glass-ceramics. *AM Ceram Soc.* 68:112-119, 1985.

[54] M.E. EBRAHIMI, J. CHEVALIER and G. FANTOZZI. Slow crack-growth behavior of alumina ceramics Materials. 15:142-147, 1999.

[55] M. CICCOTTI, G. GONZATO and F. MULARGIA. The double torsion loading configuration for fracture propagation: an improved methodology for the load-relaxation at constant displacement. *Rock Mechanics and Mining Sciences*. 37:1103-1113, 2000.

[56] J. CHEVALIER, A.H. DE AZA, L. GREMILLARD, R. ZENATI and FANTOZZI G. Slow crack growth in zirconia ceramics: from the single crystal to the composites. *Mater Eng.* 12:159-178, 2001.

[57] D.J. GERRY and J.O. OUTWATER. On the fracture energy, rehearing velocity and refracture energy of Cast epoxy resin. *J. Adhesion*. 1:290-298.

[58] J.A. KIES and A.B.J. CLARK. Fracture propagation rates and times to fail proof stresses in bulk glass. In: P. L. Pratt, editor. Proceedings of the second International Conference on Fracture, Brighton, England. London: *Chapman and Hall Ltd*. 483-491, 1969.

[59] D.P. WILLIAMS and A.G. EVANS. A simple method for studying slow crack growth. *J Test Eval.* 1:264-270, 1973.

[60] P. LEEVERS. Crack front shape effects in the double torsion testing. *Journal of Material Science*. 17:2468-2480, 1982.

[61] G.G. TRANTINA and C.A. JOHNSON. Subcritical crack growth in Boron-Doped SiC. *American Ceramic Society.* 58:44, 2006.

[62] M. CICCOTTI. Realistic Finite-Element Model for the double torsion loading configuration. *J. Am. Ceram. Soc*. 83:2737-44, 2000.

[63] M. CICCOTTI, N. NEGRI, G. GONZATO and F. MULARGIA. Practical application of an improved methodology for the double torsion load relaxation method. *Int J Rock Mech Min Sci.* 38:569-576, 2001.

[64] G. VENKATACHALAM, R. HARICHANDRAN, S. RAJAKUMAR, C. DHARMARAJA and C. PANDIVELAN. Determination of j-integral and stress intensity factor using the commercial FE software ABAQUS in austenitic stainless steel (AISI 304) plates. *Int J Adv Manuf Technol.* 2008.

[65] S. COURTIN, C. GARDIN, G BÉZINE and B.H HAMOUNDA. Advantages of the j-integral approach for calculating stress intensity factors when using the commercial finite element software Abaqus. *Engineering Fracture Meachnics*. 72:2174-2185. Elsevier Science Ltd, 2005.

[66] N. KAMP, M.R. PARRY, K.D. SINGH and I. SINCLAIR. Analytical and finite element modeling of roughness induced crack closure. *Acta Mater* 52(2):343-353, 2004.

[67] G. G. TRANTINA. Stress analysis of the double-torsion specimen. *Journal of the American Ceramic Society*. 60(7-8):338–341, 1977.

[68] M. A. MADJOUBI, M. HAMIDOUCHE, N. BOUAOUADJA, J. ChEVALIER, and G. FANTOZZI. Experimental evaluation of the double torsion analysis on soda-lime glass. *Journal of Materials Science*. 41(18):7872–7881, 2007.

[69] R.B. TAIT, P.R. FRY and G.G. GARRETT. Review and Evaluation of the Double-Torsion Technique for Fracture Toughness and Fatigue Testing of Brittle Materials. *Experimental Mechanics*. 15:14-22, 1987.

[70] H.L. EWALDS and R.J.H. WANHILL, Edward Arnold, London. 304 pages, illustrated, paperback. 1984.

[71] M. JANSSEN, J. ZUIDEMA and R.J.H. WANHILL. Fracture mechanics 2nd Edition. Delft DUP Blue Print. 2002.

APPENDIX A

Abaqus Implementation of Conventional FEM

In Abaqus, the model was created to be similar to the one that was created by Rosie at al. [7]. The specimen's dimensions are given in Table (3).

	CT	DTDCB
W	50mm	50mm (front)
B	8mm	24.2mm
L	75mm	215.9mm
h	-	152.4mm
θ	-	73.3^{o}

Table A.1. CT and DTDCB specimen dimensions

A.1.1 Model Creation:

The CT specimen or DTDCB specimen models had the same mechanical properties but different design lengths:

- Modelling space: 3D;
- Type: Deformable; and
- Shape: Solid.

Abaqus created a part as the defined specimen.

A.1.2 Loading Pin:

The loading pin is modeled as the one that is an analytical rigid part, i.e the deformation does not form part of the analysis and is modelled in the reference pin.

- Modelling space: 3D; and
- Type: Analytical rigid shell.

A.1.3 Assembly:

The assembly section was used to link the two models, CT/DTDCB specimen and the loading pin. Both of these models were treated as independent. This was to allow us to have a simple and a clear meshing part to the specimens, except the loading pin, which did not form part of the model.

A.1.4 Step:

A step was created on the step module and was set to be static general, in order to allow the crack tip to be easily identified.

A.1.5 Mesh:

After the model was assembled, the mesh was created earlier in order to partition the model appropriately.

- Elements: Linear hexahedron
- Type: C3D8R

A.1.6 Crack:

Under the interaction module, create, under **Special**, a crack with a contour integral as the type. The crack front was selected, and the direction was set to q −vectors from (0,0,0) to (1,0,0) a s t he di rection in w hich the c rack w ould pr opagate. T his di rection i s i n t he x −axis, perpendicular to the load experienced by a specimen.

- Symmetry Plane: half crack model,
- Singularity, midside node parameter: 0.25,
- Collapsed element side: single node.

A.1.7 History:

Output Request

- Domain: Contour integral, select the crack to process n = 1,
- Number of contours: 15,
- Type: Stress intensity factors.

A.1.8 Interaction

- Type: Surface to surface contact,
- Step: The step that was created (static, general).
- Master: Analytical rigid, loading pin.
- Slave: Specimen
- Sliding formulation: finite sliding
- Description method: Surface to surface
- Contact interaction property:
  - Type - Contact
  - Mechanical: Normal behavior, Adjust only to remove overclosure.

A.1.9 Loads:

A load of $7kN$ was applied to the CT specimen, and the load of $11kN$ was applied to the DTDCB specimen for comparison to the literature.

A.1.10 Boundary Conditions:

Symmetric boundary conditions were applied to the $y-$direction, starting at the crack tip. We fixed the $z-$ direction, so that the specimen did not move sideways, and the pin boundary condition was applied, so that the pin was only allowed to move in the $y-$direction.

A.1 Abaqus Implementation of EXtended FEM

The preliminary factor that should be taken care of in the XFEM is the use of maximum principal stress. The physical model was created in the Part module in Abaqus. The specimen shown in Fig (B.1) was created as the physical model. It consists of the following:

A.2.1 Part: Fig. (B.2)

CT and DTDCB specimen:

- Modeling space: 3D,
- Type: Deformable

  Solid part(1 cell, 18 solid faces, 46 edges, 32 vertices)

A.2.2 Loading Pin

- Modeling space: 3D,
- Type: Analytical rigid

Shell part(1 shell face, 3 edges, 2 vertices)

A.2.3 Crack

- Modeling space: 3D,
- Type: Deformable

Shell part(1 shell face, 4 edges, 4 vertices)

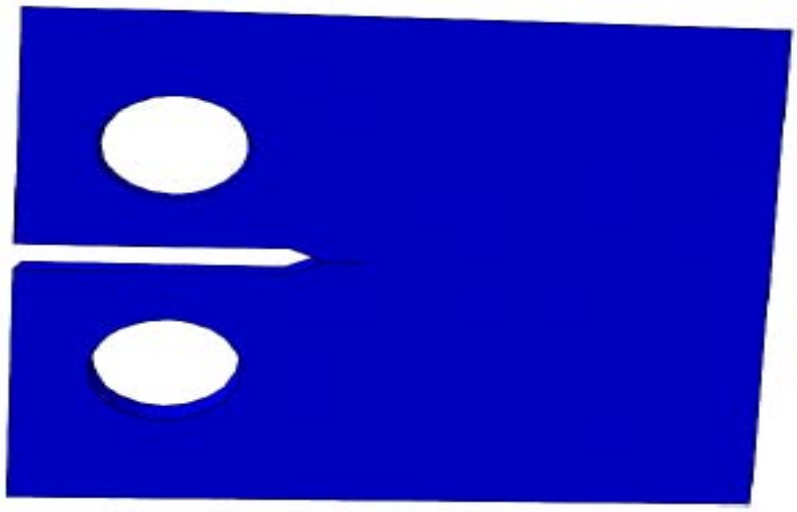

Figure A.1. Initial Crack for the CT specimen.

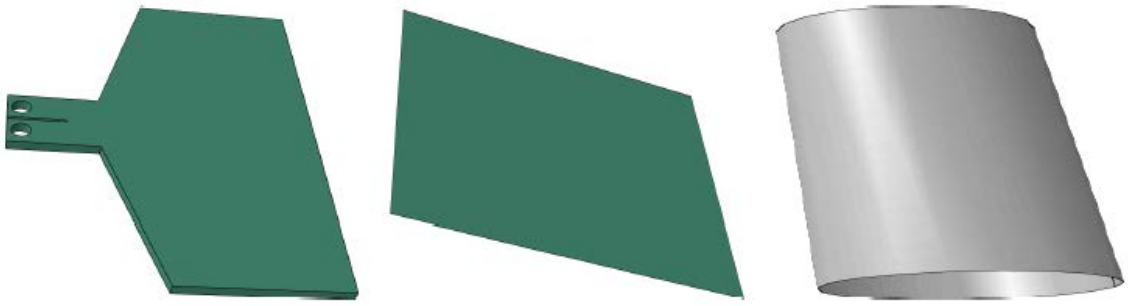

Figure A.2. DTDCB specimen, a crack shell and an analytical rigid Pin

A.2.4 Material Properties:

Mild steel Properties:

- Young modulus: 207GPa
- Poison's ratio: 0.33
- Maxps Damage: Max Principal stress: 220MPa
- Maxps Damage Tolerance: 0.1 (not material property, but it is used to allow convergence with the XFEM method)
- Damage evolution
    * Softening: Linear
    * Degradation: Maximum
    * Mixed mode behavior: Mode-independent
    * Mode mix ratio: Energy
    * Fracture energy: 42200

A.2.5 Step:

Create a static general step in the step module and include large displacement effects (**NLgeom** toggled on).

A.2.6 Propagating Crack

Define crack geometry (if initial crack is present) and the crack domain. Note that the crack has no mechanical properties, since it does not form part of the analysis. It was only included to describe the crack location. Position the crack at the correct crack position, but this is not a limitation, since cracks in materials can propagate anywhere, if the stresses are high.

The following should be included in XFEM simulation to ensure that the crack does propagate. This is supported in Abaqus.

1. Field Output Request

- Under State/Field/User/Time

  * STATUSXFEM, Status of xfem element

- Under Failure/Fracture

  * PHILSM, Level set phi

- Interactions

  * Upper/Bottom Pin
    - Master surface = loading pin
    - Slave surface = TDCB specimen

  * Sliding formulation: Finite sliding

  * Discretization method: Surface to surface

  * Slave adjustment: Adjust only to remove over-closure.

  * Contact interaction property: Create mechanical contact as the normal behavior

  * Create interaction of XFEM crack growth as a type and toggle on allow crack growth in this step.

A.2.7 Mesh

Only first-order solid continuum stress/displacement elements can be associated with an enriched feature. For propagating cracks, these include bi-linear plane strain and plane stress elements, linear brick elements, and linear tetrahedron elements. For stationary cracks, these include linear brick and linear tetrahedron elements.

- Total number of elements: 24072
- 24072 linear hexahedral elements of type C3D8

APPENDIX B

Abaqus Modelling of the DT specimen

The following is the list of procedures that were followed during the modelling process of the DT geometry. It is worth noting that the steps listed here may not necessarily need to be followed as listed.

B.1.1 Part

Solid Part
Modelling space 3D
Type: Deformable

B.1.2 Material Property

PMMA properties
(Young modulus, 3720 and Poisson's Ratio 0.328)

B.1.3 Crack Type

Contour integral
Q-vectors (0,1,0)
Seam crack
Mid-side node parameter ($0 < t < 1$): 0.5

B.1.4 History Output

Domain: Crack

Select the seam crack

Stress Intensity factors

Maximum energy release rate

B.1.5 Interaction

1. Self-Contact (between cracked surfaces)

   Surface-to-Surface
   Static, General Step

2. Surface-to-Surface Contact (between c racked s urfaces, to p revent overlap)

B.1.6 Contact Property Options

Friction formulation: Penalty

Friction Coefficient: 0.5

Normal Behaviour “Hard contact”

B.1.7 Constraints (between the loading surfaces and the specimen)

Type: Tie, and Rigid body

4 in total (2 constraints and 2 Rigid Bodies)

B.1.8 Boundary conditions and Loads

Left and right loads

Type Moment: 0.5 (both sides, but opposite directions)

Left Moment: CM 1= 0

CM 1= -0.5

CM 1= 0

Right Moment: CM 1= 0

CM 1= 0.5

CM 1= 0

Back: $U_1 = U_3 = 0$

Loading points: $U_3 = 0$

B.1.9 Mesh

Quadratic hexahedral elements of type C3D20 (Specimen)

Linear quadrilateral elements of type R3D4 (Crack tip)